Biophysical Reviews
https://doi.org/10.1007/s12551-019-00601-7

REVIEW

Continuous noninvasive glucose monitoring; water as a relevant marker of glucose uptake in vivo

Andreas Caduff[1] · Paul Ben Ishai[2] · Yuri Feldman[1]

Received: 30 May 2019 / Accepted: 13 October 2019

Abstract
With diabetes set to become the number 3 killer in the Western hemisphere and proportionally growing in other parts of the world, the subject of noninvasive monitoring of glucose dynamics in blood remains a "hot" topic, with the involvement of many groups worldwide. There is a plethora of techniques involved in this academic push, but the so-called multisensor system with an impedance-based core seems to feature increasingly strongly. However, the symmetrical structure of the glucose molecule and its shielding by the smaller dipoles of water would suggest that this option should be less enticing. Yet there is enough phenomenological evidence to suggest that impedance-based methods are truly sensitive to the biophysical effects of glucose variations in the blood. We have been trying to answer this very fundamental conundrum: "Why is impedance or dielectric spectroscopy sensitive to glucose concentration changes in the blood and why can this be done over a very broad frequency band, including microwaves?" The vistas for medical diagnostics are very enticing. There have been a significant number of papers published that look seriously at this problem. In this review, we want to summarize this body of research and the underlying mechanisms and propose a perspective toward utilizing the phenomena. It is our impression that the current world view on the dielectric response of glucose in solution, as outlined below, will support the further evolution and implementation toward practical noninvasive glucose monitoring solutions.

Keywords Glucose monitoring · Dielectric spectroscopy, Impedance spectroscopy · Microwave · Water · Cole–Cole broadening · Multisensor

Introduction

Diabetes mellitus is a disorder caused by insufficient or nonproduction of the hormone insulin by beta cells in the pancreas (Mensing et al. 2004). It has essentially two negative side effects on the body that act on different time scales (Brownlee 2005; Nathan 2014). The short-term side effect, called hypoglycemia, is triggered by low concentrations of glucose in the blood and can typically lead to reduced motor control, loss of consciousness, or even seizures. Therefore, it is greatly feared by many diabetes patients. The long-term side effect is the negative impact of extended exposure to high levels of glucose concentration in the blood, called hyperglycemia. This can lead to permanent damage of a variety of body functions, including nephropathy (kidney damage) and retinopathy (retina). To avoid these two conditions, patients with insulin-dependent diabetes need to carry out self-monitoring of their blood glucose levels (SMBG), often via invasive and regular daily blood sampling. Unsurprisingly, there is a tremendous interest in finding a cost-effective method of noninvasive and continuous blood glucose monitoring (NIGM).

An increasingly popular and powerful option is needle-based continuous glucose monitoring systems (CGM). CGM systems require a glucose oxidase–loaded needle to be placed in the subcutaneous tissue (Garg and Akturk 2018; Rodbard 2016; Wadwa et al. 2018). Such systems are often placed abdominally or on the upper arm, which seems to become an increasingly popular location for the attachment of medical devices per se. Obviously, these systems are still invasive, and the sensor must be regularly changed. Despite these limitations, there is a substantial body of evidence that shows the benefit of CGM in different patient settings (Danne et al.

✉ Yuri Feldman
yurif@mail.huji.ac.il

[1] Applied Physics Department and the Center for Electromagnetic Research and Characterization, The Hebrew University of Jerusalem, 91904 Jerusalem, Israel

[2] Department of Physics, Ariel University, 40700 Ariel, Israel

Published online: 18 November 2019

2017; Schrangl et al. 2018). To address the foreign body reaction by reduction of total needle surface, microneedle-based systems have recently been proposed (Lee et al. 2016; Ribet et al. 2017).

The availability of a truly noninvasive-based sensor system that provides diabetic patients with continuous readings of their glucose variations and levels would have a tremendous impact on their quality of life by permitting easier control of those same levels.

Over the last four decades, several noninvasive glucose monitoring approaches have been studied, including spectrophotometric (IR light, fluorescence bases, etc.), electrical impedance, photoacoustic, light scattering, dielectric spectroscopy (DS) (or impedance spectroscopy), as well as combinations thereof, and wearable electrochemical sensors (Ascaso and Huerva 2016; Caduff and Talary 2015; Chowdhury et al. 2016; Jintao et al. 2017; Lilienfeld-Toal et al. 2005; Vashist 2012; Yadav et al. 2015). They are focused not only on the microvascular blood in the skin and underlying tissue, but also on electrochemical sensors to sample saliva (Aguirre et al. 1993), tear fluid (Yan et al. 2011), sweat (Windmiller and Wang 2013), and interstitial fluid (Tierney et al. 2001) for ex vivo processing. These approaches (except the last one) can provide a painless procedure for the determination of glucose concentration. Some of these methods are minimally invasive, while some are not continuous. However, none are truly convenient to the user. As for the direct determination of blood sugar levels, all methods work through skin measurements. They are susceptible to perturbations arising from extrinsic (e.g., environmental) and intrinsic (e.g., effect of endogenous hormones) effects and from variations between subjects, such as physical state, blood pressure, skin hydration, blood perfusion, skin chemistry, temperature, or skin pigmentation (Caduff and Talary 2015). A summary of such perturbations, particularly blood perfusion, has been presented earlier (Caduff et al. 2010).

The main difficulty with the various spectroscopic methods, such as infrared spectroscopy, is the relatively weak changes in the registered signals due to changes in the glucose concentration. This leads to limited resolution capability and insufficient precision, particularly under less controlled conditions where other physiological dynamics can be superimposed on the effective glucose signal (Caduff et al. 2003a). Several studies have been performed with multisensor systems that combine DS with other sensing capabilities to arrive at more robust NIGM that may offer initially indications in glucose trends. Increasingly, these solutions are in combination with other physiological monitoring capabilities (Caduff et al. 2015, 2018; Zanon et al. 2013a, b, 2018).

Of the above numerated methods outlined above, DS and the related technique of impedance Spectroscopy stand out. Up to 2 GHz, the experimental techniques for measuring the dielectric permittivity or the impedance of a sample are almost indistinguishable, as both relate to the sample as a lumped element having a macroscopic impedance in an electrical circuit (Kremer and Schonhals 2003; Raicu and Feldman 2015). However, by the application of the relationship $\varepsilon^*(i\omega) = 1/(i\omega C_0 Z^*(i\omega))$, where $\varepsilon^*(i\omega)$ is the complex dielectric permittivity, $Z^*(i\omega)$ the complex impedance of the sample, C_0 the geometric constant relating to the shape and size of the sample, and ω the cyclic frequency, dielectric spectroscopy is able to open a window on the molecular level of relaxation and interaction in the sample. Above 2 GHz, it becomes difficult to consider the sample as a simple lumped element and one must consider instead the reflection or transmission coefficient of the material under test, depending on the dielectric strength involved (Feldman et al. 2006a; Raicu and Feldman 2015). Consequently, among the numerous modern methods used for materials analysis, dielectric spectroscopy is unique in its ability to investigate the relaxation processes of complex biological systems in an extremely wide frequency interval (10^{-1}–10^{12} Hz) (Beving et al. 1994; Grant et al. 1978; Kuang and Nelson 1998; Pethig 1977, 1979; Schwan 1957, 1963; Takashima 1989; Wolf et al. 2011). The study of the dielectric properties of biological systems and their components is important not only for fundamental scientific knowledge but also for applications in medicine, biology, biotechnology, and physiology (Raicu and Feldman 2015). Biological systems typically consist of hierarchical layers of complexity—from protein or DNA solutions to cell suspensions, colonies, or tissues. The analysis of their complex dielectric spectra allows one to obtain physical parameters of macromolecular conformations or of different cell compartments. For example, one can calculate the conductivity and permittivity of the cytoplasm and of the interior of cell organelles, or the capacitance, conductance, porosity, and surface properties of the various cell membranes (Feldman et al. 2003; Gabriel et al. 1996; Hayashi et al. 2003, 2008; Raicu and Feldman 2015; Takashima 1989). Consequently, DS or impedance spectroscopy has been actively used for the last two to three decades to investigate and build NIGM sensors in a wide frequency band from kilohertz to gigahertz (Caduff et al. 2003a; Forst et al. 2006; Huang et al. 2019; Pfutzner et al. 2004; Talary et al. 2006) and increasingly to microwaves (Nikawa and Someya 2001; Siegel et al. 2014, 2015, 2016; Tierney et al. 2001; Xiao and Li 2017). Very recently, Zhang et al. reviewed the state of art in NIGM technology, particularly focusing on optics and terahertz frequencies, while Yilmaz et al. reviewed DS-based approaches including microwaves (Yilmaz et al. 2019; Zhang et al. 2019).

Almost all reported work has used DS for in vitro measurements of glucose concentrations in model systems and as a calibration for their own sensor idea (Huang et al. 2019). Some of the research and development groups went further and applied their sensors for in vivo measurements both on animals (Siegel et al. 2014, 2015, 2016) and on human

(Caduff and Talary 2015; Choi et al. 2015; Guarin et al. 2013). Even though much work has been done in exploring basic questions of mechanism, the sensitivity of DS to glucose concentration is routinely ignored.

In this review, we primarily address this fundamental question: "Why is dielectric or impedance spectroscopy sensitive to changes of glucose concentration in the blood and why can this be done over a very broad frequency band, including microwaves?"

The question is more subtle than it appears because the glucose molecule, despite having a dipole moment of 8.7 D, is usually screened by its hydration shell. In solution, its contribution to the response from molecular tumbling should not be noticeable (Caffarena and Grigera 1999; Kaatze 1990; Levy et al. 2012a). Yet it is extremely amenable to dielectric probing.

Below we will attempt to answer this question, in the different frequency bands, where NIGM sensors have been tried in recent decades.

The initial hypothesis: β dispersion?

The nomenclature of dielectric dispersion of biological tissues was first designated by Schwan (1957). In general, the permittivity decreases with increasing frequency and can be divided into three major regions (i.e., dispersions), known as α, β, γ, and a further subsidiary dispersion, known as δ (see Fig. 1).

The α relaxation process is observed mainly in the low-frequency region, below 10 kHz. This dispersion is the result of the slow migration of ions or deformation of ion clouds at the expansive surface cell membranes or tubular systems, such as the sarcoplasmic reticulum in muscle fibers or along DNA molecules (Asami 2014; Gabriel et al. 1996; Pethig and Kell 1987; Schwan 1957; Takashima 1989). The β dispersion

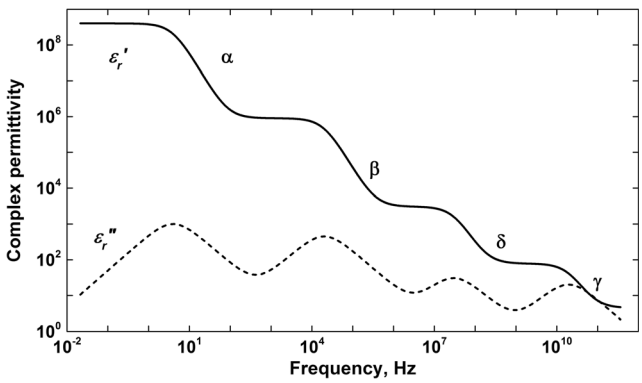

Fig. 1 Schematic view of the dielectric permittivity (solid line) and loss (dashed) spectrum of a typical biomolecular aqueous solution (Raicu and Feldman 2015; Schwan 1957). Typically, four relaxations can be noted. Using the nomenclature of the figure, these are as follows: α is related to ionic mobilities, β is related to interfacial polarizations of cellular structures, and γ is the iconic relaxation of bulk water. The source of the intermediate δ is still a point for scientific debate

usually occurs in the range of 0.l–10 MHz (Asami 2002a; Schwan 1957) and is related to the cellular structure of tissues, whose poorly conducting membranes separate the cytoplasm and extracellular space, each with different dielectric properties. The polarization of these cellular membranes leads to a large frequency-dependent permittivity. This is also known as a Maxwell–Wagner polarization (Raicu and Feldman 2015; Schwan 1957). The γ dispersion is due to the relaxation of free water, and its maximum is observed in the microwave frequency region, around 25 GHz at 37 °C (the typical temperature of living tissue) (Grant et al. 1978; Pethig 1977; Raicu and Feldman 2015). Between the β and γ dispersions in the dielectric spectrum, another subsidiary process is observed, which is denoted as the δ dispersion. The molecular origin of the δ relaxation has been subject to theoretical and experimental research for the last three decades, but still remains unclear (Feldman et al. 2014; Schwan 1957; Wolf et al. 2015).

To understand the sensitivity and characteristics of impedance sensors for noninvasive glucose monitoring, it helps to consider the dielectric response of glucose in the blood within this framework (Caduff et al. 2003a, 2006). One of the earlier impedance sensors successively applied for in vivo NIGM was designed as a fringing capacitance attached to the skin and operating in the frequency range from 20 to 50 MHz. This range can be assigned to the right (high frequency) wing of the β dispersion (Caduff et al. 2003a; Caduff and Talary 2015). With an observed correlation between the temporal evolution of the sensor signal and the dynamics of glucose in the blood, it was assumed that the sensor was capable of recording the impact of a glucose variation on the impedance changes in the body related to blood (Caduff et al. 2003a, 2006). Consequently, red blood cells (RBC), or erythrocytes, were considered one of the possible candidates for the verification of this hypothesis, as these are the major cellular component of blood (Hayashi et al. 2003). Erythrocytes are non-nucleated cells and consist simply of a cell membrane and cytoplasm. Like other cell membranes, the RBC membrane is a fluid-like structure composed of a semipermeable lipid bilayer with an asymmetrically organized mosaic of proteins. Its characteristic biconcave disc shape provides a surface area to volume ratio that is optimal for gas exchange. Throughout the course of their lifespan, the cells are exposed to shear force as they navigate the narrow capillaries and hence need to undergo rapid, reversible deformations. To cope with this stress, the RBC is equipped with a specialized cytoskeleton that provides the mechanical stability and flexibility necessary to withstand these forces. The membrane is thus composed of various transmembrane proteins and a filamentous meshwork of proteins that forms a skeleton along the entire cytoplasmic surface of the membrane. The most abundant protein in the membrane skeleton is spectrin, with different transporters that serve different purposes such as for ion exchange, glucose transport, or water migration (Stokke et al. 1986).

The dielectric properties of erythrocytes are nevertheless not straightforward (Hayashi et al. 2008) because of their non-spherical, biconcave shape (see Fig. 2).

However, while the papers (Caduff et al. 2003a, 2006) reported a sensitivity to blood glucose dynamics, DS cannot directly be sensitive to glucose. Intuitively, one would expect a glucose-based dielectric dispersion, as polarization mechanisms in which the solute and solvent dipoles reorient almost independently. But no dispersion has ever been detected experimentally for glucose in aqueous solutions (Fuchs and Kaatze 2001). This is due to the symmetrical structure of the glucose molecule and its shielding by the water's smaller dipoles. This is particularly true for solutions of relatively low glucose concentration, that are physiologically relevant (Fuchs and Kaatze 2001; Levy et al. 2012a). The implication was that all DS measurements demonstrating a sensitivity to glucose variations are recording it indirectly. Hence, they are looking at a secondary effect caused by the variation of glucose. The mechanism of this sensitivity was unclear and numerous investigations over more than a decade of in vitro RBC suspension studies have been carried out. These are involving glucose experiments with and without blocking its selective transporter GLUT1, and fructose experiments with its selective transporter GLUT5, various ATP experiments with regular RBC, and ghost cells or the implications of spherically versus biconcave-shaped RBC (Hayashi et al. 2003; Livshits et al. 2007, 2009) were carried out in order to elucidate the nature of DS sensitivity to changes in glucose levels. Some aspects of these experiments and its results will be further discussed below.

The cells of organisms require energy to maintain their normal function, and one of the major fuel resources is D-glucose. Because mature erythrocytes lack both nuclei and mitochondria, they are incapable of generating energy via the oxidative cycle. Instead, erythrocytes depend on the anaerobic conversion of glucose for the generation and storage of high-energy phosphates, such as adenosine-5′-triphosphate (ATP) (Heard et al. 2000; van Solinge and van Wijk 2010). Not surprisingly, ATP is called the "universal energy carrier" or "energy currency" of cells. It is well known that glucose transport through biological membranes requires specific transporter proteins. Glucose carriers or glucose transporters (GLUT) catalyze facilitated transport of sugars through the cellular membrane. GLUT transporters form aqueous pores across the membrane, through which sugars can move in a passive manner; consequently, these transporters can only transport sugars down their concentration gradient at a rate of about 50,000 times greater than transmembrane diffusion. The insulin-independent glucose transporter of erythrocytes (called GLUT1 to distinguish it from the other, including insulin-dependent–related transporters) is a membrane protein with 12 hydrophobic segments, each of which is believed to form a membrane-spanning helix (Zuo et al. 2003). The structural model of GLUT1 suggests that the side-by-side assembly of several helices produces a transmembrane channel lined with hydrophilic residues that can hydrogen bond with glucose as it moves through the channel (Fig. 3). Glucose transport and uptake is regulated by the presence of intracellular ATP, binding on the interior side to this membrane protein (Heard et al. 2000).

Fig. 2 The human red blood cell (erythrocyte). The biconcave shape of the cell leads to an asymmetric dielectric response in the β dispersion

The conformational changes of the transporter due to ATP binding are the opposite of those seen with adenosine monophosphate (AMP). The negatively charged ATP alters the tertiary structure of the GLUT1 by binding to the cytosolic endofacial vestibule, a process that inhibits the net sugar transport, and when AMP is bound, sugar transport can take place (Heard et al. 2000).

In a recent, detailed study of the dielectric response of D- and L-glucose uptake by biconcave RBC in vitro (Hayashi et al. 2003; Livshits et al. 2007, 2009), the dielectric spectra of biconcave cells were analyzed using the spheroid shell model (Asami 2002b; Asami and Yonezawa 1995). From this model, the specific membrane capacitance C_m of a single biconcave erythrocyte was calculated. Complementary experimental methods proved that the RBC size is independent of D-glucose concentration (Hayashi et al. 2003). Finally, it was shown that the C_m is strictly dependent on the D-glucose concentration (Fig. 4). In contrast, no correlation was found between the membrane capacitance and the L-glucose concentration (Livshits et al. 2007, 2009).

It was proven that the dielectric response of RBC to D-glucose uptake depends on the efficiency of the glycolysis and its regulation by the resulting product, ATP, and its specific interaction with the main D-glucose transporter GLUT1 (Livshits 2007). Due to the significant number of transporters

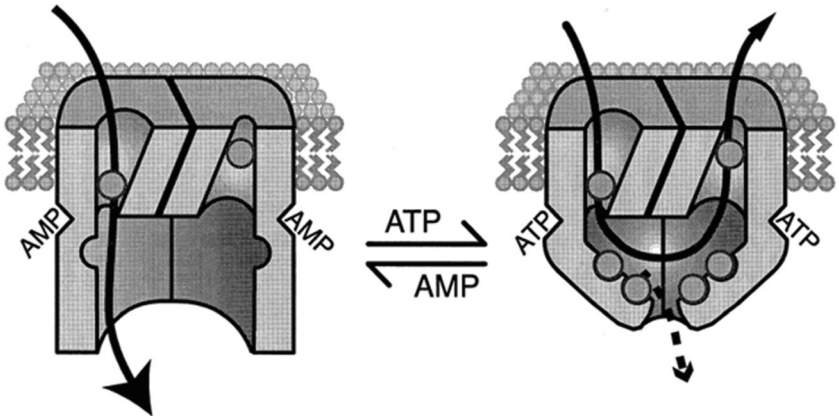

Fig. 3 Model for GLUT1-mediated transport (adapted from Heard et al. 2000)). The figure to the left shows a substrate transported through GLUT1. In the absence of ATP or when AMP is bound to GLUT1 (left), sugar can cross easily into the cell. Upon ATP binding (right), a conformational change occurs that restricts sugar transport

per cell membrane surface area, glucose uptake affects the total membrane polarization and, consequently, the dielectric properties of the membrane.

The first generation of measurement system, where DS has been applied as a method for noninvasive glucose monitoring, showed reasonably strong sensitivity to different environmental conditions and to the subject's physiological state. Even with these caveats, it was shown (Caduff et al. 2006; Talary et al. 2006) that a fringing field capacitive sensor could be employed in in vivo situations for glucose monitoring. The device formed a RLC resonant circuit in series when placed on the surface of the skin (see Fig. 5) (Talary et al. 2006), whereby the underlying properties of the skin, subcutaneous tissue, and capillary blood modify the values of the electrical components R and C.

It monitors the changes in the minimum of the impedance modulus in the frequency range 20–50 MHz. The aim was to correlate these variations with the blood glucose levels (Raicu and Feldman 2015). Comprehensive studies of the sensor

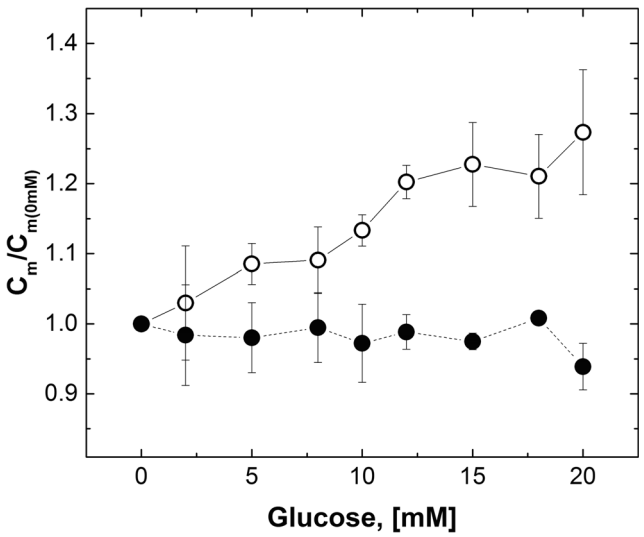

Fig. 4 The normalized cell membrane capacitance of biconcave erythrocyte suspensions versus D- (open) and L-glucose (full) concentration. C_m was normalized to 0 mM data because of physiological differences between donors. Mean values ± SD (n = 12). Reproduced with permission from Livshits et al. (2007) (Copyright 2007, IOP)

sensitivity mechanism resulted in several attempts (Caduff 2004; Livshits 2007) to establish whether the observed alterations of the skin and underlying tissue dielectric properties could be correlated to the concentration of blood glucose. Underlying the first generation of NIGM was the idea that there would be sensitivity to changes in the interfacial polarization of β dispersion, due to the change of electrolyte balance across the cells in the blood and underlined tissues, as a result of changes in glucose concentration (Caduff et al. 2003b). For this reason, the working frequency interval of DS-based NIGM devices was chosen between 20 and 50 MHz (Caduff et al. 2011; Caduff and Talary 2015). However, it became rapidly evident that the condition of the skin was individually variable and critical to the passage of the signal to the dermal layers of capillary blood. Consequently, multisensory approaches to NIGM began to be employed. It was clear that the readings followed the variation of glucose concentration, but significantly depended on the condition of the skin, its temperature, the variability of the morphology of the different skin layers, blood perfusion or sweat, etc. (Abe et al. 2008). Furthermore, the expected efficiency of DS to detect variations of glucose concentration in the megahertz frequency range was faced with a number of challenges when a DS (or impedance) sensor was applied in vivo. The main contradiction encountered during in vitro measurements of the dielectric properties of the RBC suspensions, as compared to in vivo measurements, was a reverse tendency of the alteration in dielectric properties with the change in glucose concentration. While the dielectric permittivity (or capacitance) of the RBC membrane in vitro increased with glucose uptake, the in vivo results showed the opposite behavior.

Fig. 6 shows a representative example for a trial day, comparing the change in dielectric properties of the skin and the underlying tissue of a subject, with varying in vivo glucose levels over time (Dewarrat et al. 2011). It is clear that the decrease in blood glucose concentration leads to the increase of the dielectric properties of the dermis obtained by a prototype NIGM sensor attached to the subject's arm. The reason for the opposite behavior of the parameters measured in vivo to that of the in vitro study was a question for debate.

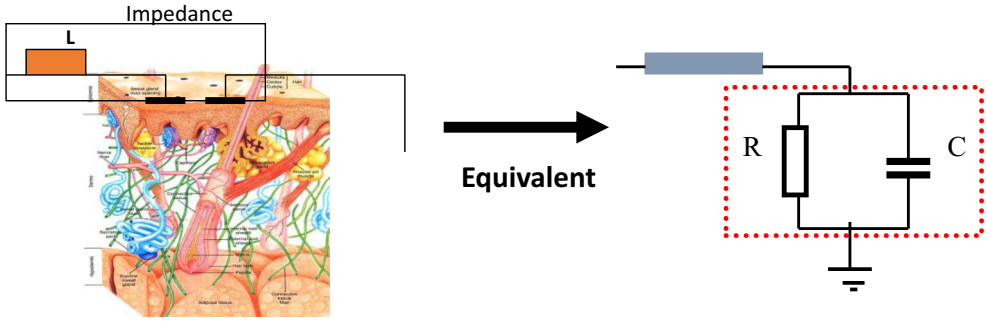

Fig. 5 Equivalent circuit of an initial fringing field capacitive sensor coupled to skin. In this simplified model, *R* represents the surface resistance of the skin and *C* the capacitance of the skin under the electrodes

One of the strategies used to resolve the problem was to extend the frequency range of DS monitoring. A specific experiment was performed using broadband time domain DS (TDDS) with a standard fringing capacitance coaxial sensor attached to a subject's skin. The TDDS system provided readings in the time interval from 200 ps up to 4.5 μs, corresponding to the frequency range 220 kHz–5 GHz in a single measurement (Feldman et al. 2003). Surprisingly, it was found that the sensitivity of the signal to the change in glucose levels was well pronounced at 2 and 3 ns, as seen in Fig. 7, where the sensor signal (i.e., the capacitor charge) versus the time of glucose variation protocol (blue points) is demonstrated. The nature of this measured response and the sensitivity at so high a frequency can be explained only by the contribution of water. The dependence of the signal value in the time domain on glucose uptake is most probably related to the change in the bulk water content in the skin, underlying tissue and blood (which decreases with increasing glucose concentration). Traditionally, the water present in biological tissues has been defined as bound or free water, depending upon its proximity to neighboring macromolecules, membranes, or other interfaces (Feldman et al. 2014).

However, these terms are relative; as pointed out earlier, in free water, the molecules form part of a hydrogen-bonded network with each bond having an energy of around 20 kJ/mol. Such bonds must be broken before the water molecule can participate in a cooperative relaxation process, which occurs at around 18 GHz at 20 °C (Kaatze 1989). For the water molecules adjacent to a biological macromolecule as an organized hydrated layer, a so-called ice-like structure, the relaxation rate is expected to be significantly different from that of bulk water. Furthermore, in numerous studies of the dielectric relaxation of water in aqueous solutions of ionic or nonionic molecules, a symmetrical broadening of the main dielectric dispersion is always evident and usually described by the Cole–Cole (CC) law (Fuchs and Kaatze 2001; Hayashi et al. 2002; Noertemann et al. 1997; Rodríguez-Arteche et al. 2012; Ryabov et al. 2002; Shinyashiki et al. 1998). The complex dielectric spectrum of an RBC suspension (Kaatze 1990) also shows the same CC dispersion behavior (see Fig. 8). Consequently, the CC parameters of the main water peak can be considered as markers that can clarify the way and rate, at which water interacts with the different bioactive compounds in aqueous solutions.

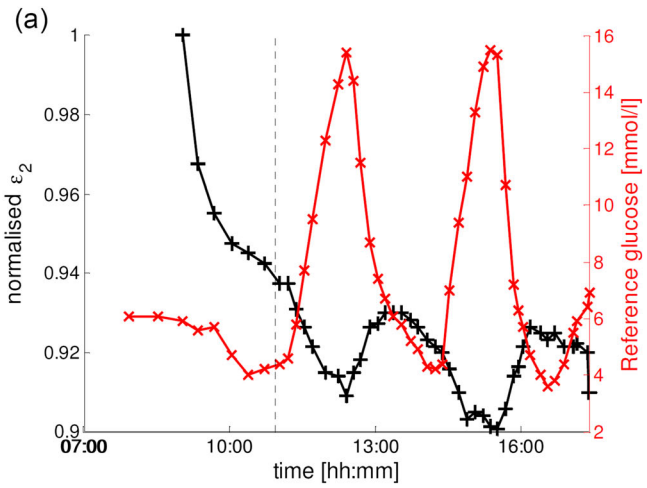

Fig. 6 Example for one trial day of the normalized (initial value equal 1) ε and σ of the dermis at 30 MHz (left axis) compared to the reference glucose profile (red, x, right axis) versus time. Black +: calculated permittivity (conductivity) of the dermis. Reproduced with permission from Dewarrat et al. (2011). The results show a dependence of the skin permittivity on the glucose concentration in the blood. However, the results obtained per subject were heavily dependent on the state of the skin, the subject, blood perfusion in the skin layer, and other factors

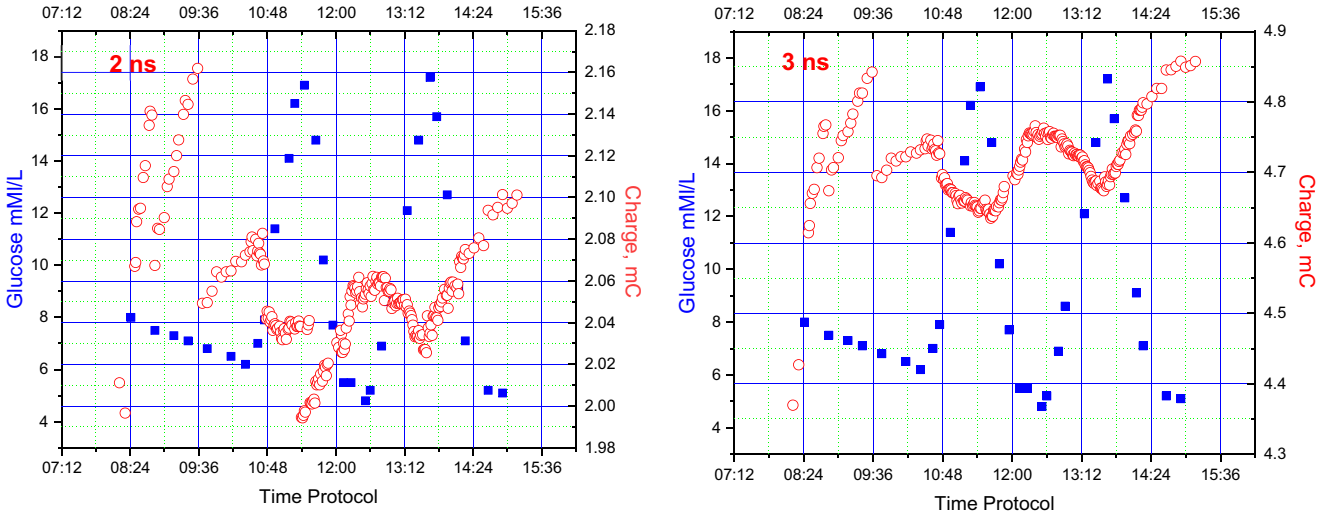

Fig. 7 The value of the capacitor charge at 2 ns (~ 500 MHz) and 3 ns (~ 330 MHz) versus time of the glucose protocol for a single subject. The results were obtained by time domain dielectric spectroscopy, using an open-ended coaxial probe attached to the subject's skin. The behavior of charge across the probe face mirrors the induced blood glucose concentration

Following these experimental observations, we will consider now the primary physical mechanism that allows us to use DS as the pivotal method for NIGM.

The basic physical mechanism underlying the main hypothesis

The properties of water are the crucial element underpinning the mechanisms of life. Yet it is a deceptively simple molecule. The key to this seeming conundrum is its affinity to form H-bonds, giving rise to 64 anomalies in its behavior (Bagchi 2012; Chaplin 2000). It would be fair also to say that our understanding of the ability of water to solvate or interact with large biomolecules is still rudimentary. The levels of complexity are only multiplied when one considered the water's role in the interface and the structures it can form therein. Of fundamental importance in this discussion is the concept of the dynamic cluster. These mesoscopic structures are short lived, yet give rise to longer-range correlations and cooperative effects. In the case of water, they are mediated by the tendency to form up to four H-bonds, leading to a local tetrahedral structure. It is also by the same mechanism that water interacts with biomolecules. Clearly, the longevity, local structure, and fluctuation of this bond must have a major impact on the functionality of these molecules (Levy et al. 2012a, b; Oleinikova et al. 2002).

One can reduce this question to a number of fundamental points as follows:

(i) The impact of H-bonded networks on aqueous solutions (Bagchi 2012; Raicu and Feldman 2015)
(ii) The influence of the H-bonded network of percolative processes and thermodynamic phase transitions
(iii) The interplay of hydration water and interface in biological activity (Oleinikova et al. 2002)

The complex permittivity spectra of bulk water can be described by the Debye function (Debye 1929; Ellison et al. 1996; Kaatze 1989):

$$\varepsilon^*(\omega) = \varepsilon'(\omega) - i\varepsilon''(\omega) = \varepsilon_\infty + \frac{\Delta\varepsilon}{1 + i\omega\tau_D}, \quad (1)$$

where ε' is the real component and ε'' the imaginary component of the complex dielectric permittivity ε^*, τ_D is the relaxation time, $i^2 = -1$, $\omega = 2\pi\nu$, ν is the frequency and $\Delta\varepsilon = \varepsilon_s - \varepsilon_\infty$ is the dielectric strength, with ε_s and ε_∞ representing the low-frequency and the high-frequency permittivity limits, respectively. This function is valid for frequencies up to 40 GHz and for most temperatures. An example of the spectra is shown in Fig. 9 for water at 25 °C (Levy et al. 2012b).

Many authors have assigned the relaxation of water, as described by the Debye function (Eq. 1), as the cumulative effect of a simple exponential (in time) relaxation of the water molecule in a viscous media, a process termed continuous rotational diffusion (CRD) (Agmon 1996). While CRD accounts reasonably well for the hydrodynamic radius of the molecule, it fails to account for the measured relaxation time, τ_D, or the dielectric strength $\Delta\varepsilon$ (Agmon 1996; Ben Ishai et al. 2015; Popov et al. 2016). Among the alternate live explanations, the wait-and-switch relaxation model based on the defect diffusion has been built and justified recently (Kaatze 2015; Popov et al. 2016). Other models have involved the relaxation of mesoscopic water clusters by various means (Ben Ishai et al. 2015). Whatever model is proposed, there is an acceptance that it is cumulative effect of these apparent moments that leads to the large dielectric response of bulk

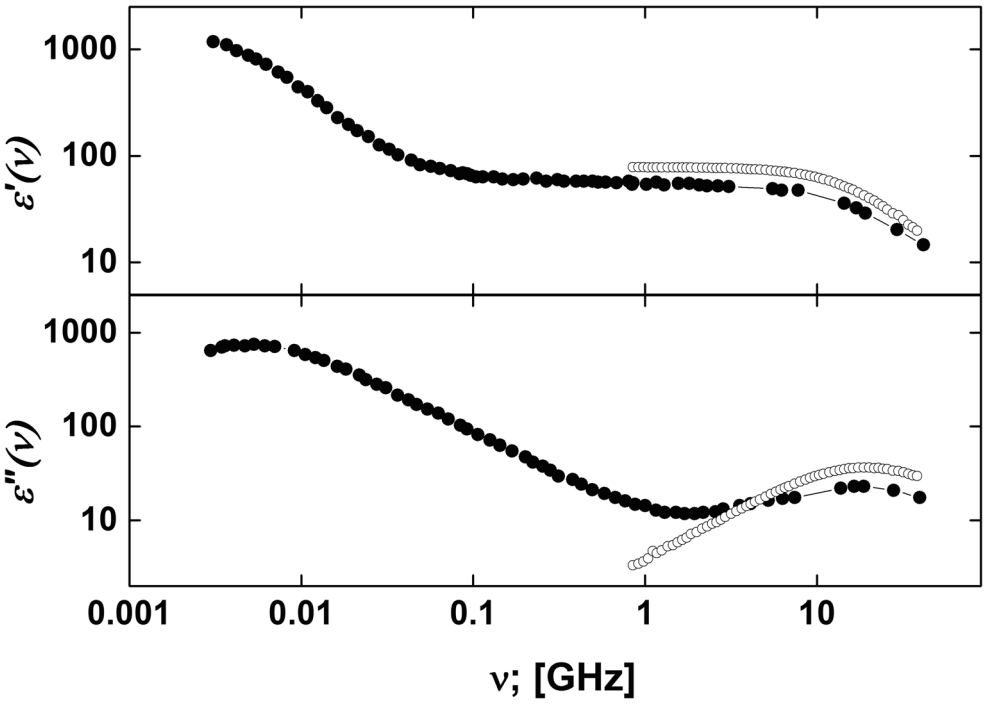

Fig. 8 The complex dielectric permittivity $\varepsilon(\nu)$, logarithmically displayed as a function of frequency, ν, for a suspension of erythrocytes in an iso-osmolar NaCl aqueous solution (filled circles, volume fraction of RBC = 0.95) and for pure water (open circles), at 25 °C. The dielectric permittivity is presented in terms of its real part, $\varepsilon'(\nu)$ and the dielectric losses $\varepsilon(\nu)$ to the negative imaginary part. The latter quantity has been derived from the total loss, $\varepsilon'' = \varepsilon''(\nu) - \sigma_{dc}/2\nu\varepsilon_0$, where σ_{dc} denotes the specific electric dc conductivity. Reproduced with permission from Kaatze (1990) (Copyright 1990, IOP)

water (Kaatze 2015; Popov et al. 2016). One point that is not disputed is that the presence of another dipole entity (charge or dipole) leads to a symmetric broadening of the peak (Feldman et al. 2013; Puzenko et al. 2010).

Water will interact with another material as either a solvent or as a solute. These could also include its role in the interface of porous materials as well as in aqueous solutions.

The broadening of dispersions linked to water in different complex systems can be described by the phenomenological CC function (Cole and Cole 1941):

$$\varepsilon^*(\omega) = \varepsilon_\infty + \frac{\Delta\varepsilon}{1 + (i\omega\tau)^\alpha}, \tag{2}$$

where α is an empirical exponent describing the loss peak broadening. Included in this, glucose or amino acids and nucleotides will also broaden the water peak once they are in the solution.

Theoretical background

In 2010, a radical departure from the traditional phenomenological approach to the parameters of the Cole–Cole equation was proposed (Puzenko et al. 2010). Based on earlier ideas that demonstrated the Cole–Cole equation as a natural result of a fractal relaxation dynamic described by the fractal Fokker–Planck equation (Coffey 2004; Coffey et al. 2006; Hilfer 2000; Metzler and Klafter 2000), it was posited that there should also be an inherent coupling between the parameters (α, $\Delta\varepsilon$, and τ) of Eq. (2). The justification for such an idea was the existence of multiple time and length scales in complex systems involving water. Clearly, any variation in composition, temperature, pressure, or other aspect of the thermodynamic state would lead to a variation of the same scales and, hence, the parameters of Eq. (2). A consideration of these parameters as a whole, rather than as phenomenological separate entities, would lead to insights in the evolution of the system.

Furthermore, posit α as an exponent of fractional time scaling, one can express it as (Puzenko et al. 2010)

$$\alpha = \frac{\ln N_\tau}{\ln(\tau/\tau_c)}. \tag{3}$$

Where τ_c is the time interval for the elementary relaxation event and N_τ is the average number of relaxation events occurring during the relaxation time τ in any mesoscopic region.

The elementary time, τ_c, can also be associated with an elementary number of acts occurring in the same mesoscopic region as before. In this case, one can express N_τ independently of the volume and apply the ideas of a recursive fractal model:

$$N_\tau = N_0 \left(\frac{\tau}{\tau_c}\right)^A, \tag{4}$$

where the mass fractal dimension A adopts values in the range $0 < A \leq 1$ (Puzenko et al. 2010). Substituting Eq. (4) in Eq. (3)

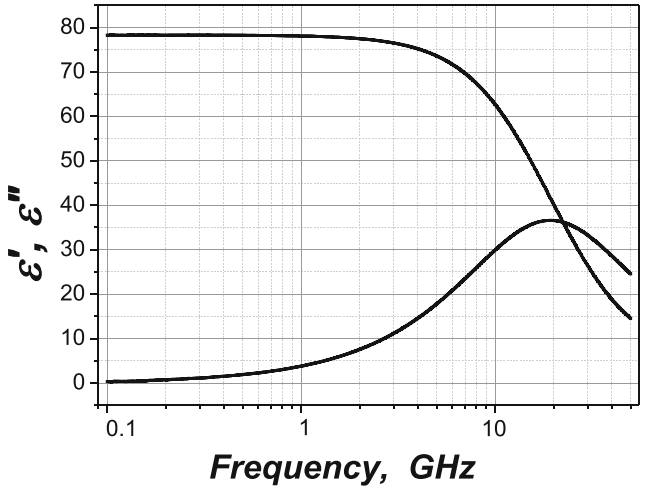

Fig. 9 The real part $\varepsilon'(\nu)$ and the imaginary $\varepsilon''(\nu)$ of the water dielectric spectra at 25 °C (1021 frequency points) (Levy et al. 2012b) (reproduced with permission from Copyright 2012, American Institute of Physics)

and introducing the new variables $x = \ln \tau$ and $x_0 = \ln \tau_c$,we can get the following relationship:

$$\alpha = A + \frac{G}{x - x_0}, \tag{5}$$

where:

$$N_0 = \exp(G), \quad \tau_c = \exp(x_0), \tag{6}$$

As a general scheme, in a complex system (CS) described by Eq. (2), the dependence of $\alpha(\ln\tau)$ can be described by a hyperbolic curve (Feldman et al. 2006b; Puzenko et al. 2010) with two asymptotes: the constant A, representing the asymptotic value of the parameter α, and the asymptote $x_0 = \ln \tau_c$. This describes two semiplanes: $\tau > \tau_c$ and $\tau < \tau_c$ (Fig. 10).

It has been observed that at a critical juncture in the system's state, one can observe a transition from one quadrant to another in the scheme described by Fig. 10 (Puzenko et al. 2012).

One cannot discuss the time evolution of a system separately from the structure in which it happens. Despite this, the inherent conceptual difficulties in doing so have led most researchers to neglect structural information ensconced in the dielectric parameters $\Delta\varepsilon$, ε_s, and ε_∞.

Fröhlich (1958) described the temperature behavior of the above parameters by the relationship:

$$B(T) = \Delta\varepsilon(T)\frac{2\varepsilon_s(T) + \varepsilon_\infty}{3\varepsilon_s(T)}T = \frac{1}{3\varepsilon_0 kV}\left\langle \boldsymbol{M}^2(T)\right\rangle. \tag{7}$$

Here, k is the Boltzmann constant, T is the absolute temperature, $\varepsilon_0 = 8.85 \times 10^{-12}$ F/m is the permittivity of free space, and V is the volume with N microscopic cells containing a dipole. $\boldsymbol{M} = \sum_{i=1}^{N} \boldsymbol{m}_i$ is the electric dipole moment of volume V and $\boldsymbol{m}_i$ is the average dipole moment of the ith volume element containing a single dipole in the same volume. The brackets in Eq. (7) indicate a statistical averaging over all possible configurations.

The significance of Eq. (7) is that the microscopic detailed sum can be evaluated by using the macroscopic dielectric parameters of Eq. (2). The same equation is valid despite the complexity of the system and even if the variation of the dielectric parameters would be by a further thermodynamic variable, such as concentration rather than temperature. Intuitively, one can recognize that the $B(T)$ function should be related to N_τ, as the number density of relaxation acts. As a visualization to this observation, it was proposed that parametric evolution of a system as a function of a thermodynamic variable, temperature per se, could be adequately described by a trajectory in a new 3D coordinate system that would span both the structural and temporal aspects of the relaxation (Puzenko et al. 2010). The coordinates of this space are $X = \ln B$, $Y = \ln \tau$, $Z = \alpha$.

Dielectric relaxation of water and its properties as a solvent

As first example of the concepts described above, glasses and clays are an excellent example of solid matrixes interacting with water. In this case, water can be viewed as dipoles that organize in different ice-like structures near hydration centers on the surface of pores in the supporting

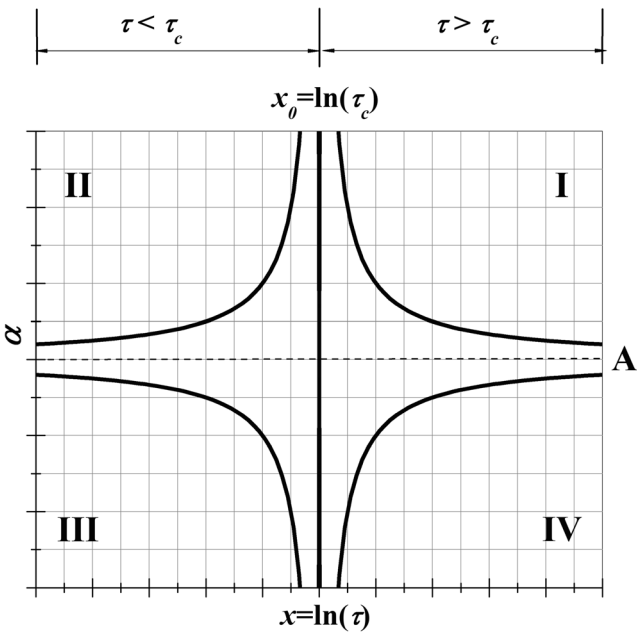

Fig. 10 The four hyperbolic branches of the function defined by Eq. (6) (Puzenko et al. 2010) (reproduced with permission from Copyright 2010, American Institute of Physics)

matrix (Feldman et al. 2014). In contrast, the broadening noted in aqueous solutions, where one could argue that water is the supporting matrix, is linked to the dynamics of the rearrangements of the H-bond network, i.e., the rearrangement of dynamic water clusters (Popov et al. 2016). This dynamic is necessarily modified in the vicinity of a solute guest molecule. One can clarify the nature of this interaction as dipole–dipole or charge–dipole.

Here, we will present results for nonionic aqueous solutions (sugars, polar amino acids) and for ionic ones (simple electrolytes, AMP/ATP, and charged amino acids). The difference in the nature of these two classifications is accentuated when exploiting the 3D trajectory approach of data presentation. Fig. 11 presents the results of a microwave (500 MHz–50 GHz) isothermal concentration study of four aqueous solutions representing different natures of solutes: glucose—dipolar (Levy et al. 2012a), NaCl—ionic (Levy et al. 2012b), ATP—a dipole with a strong negative charge (Puzenko et al. 2012), and arginine—a dipole with a weak positive charge (Levy et al. 2014).

A behavioral difference between the two types of systems (dipole–dipole or charge–dipole) is immediately obvious in the projection of the trajectories on to the $\alpha(\ln\tau)$ plane (see YZ projections in Fig.11a and11b). For glucose (dipole–dipole), $\alpha(\ln\tau)$ is located in the first quadrant ($\tau > \tau_c$; $\alpha > A$). In contrast, for ionic solutions, the curve $\alpha(\ln\tau)$ is in the second quadrant ($\tau < \tau_c$; $\alpha > A$). Complex organic molecules like nucleotides and amino acids demonstrate two features typical for both dipole and ionic solutions, depending on the concentration. Let us consider these cases separately.

Nonionic solutions

In monosaccharide solutions, the dielectric relaxation peak of bulk water is characterized by a substantially smaller static permittivity, a lower relaxation frequency, and a significant broadening (in frequency) of the relaxation peak (Levy et al. 2012a). The presence of two distinct dipoles would lead one to expect two different relaxations in the spectra, as the solvent and solute dipole reorientation almost independently of each other. However, there is no evidence for this. What one does note is that increasing monosaccharide concentrations lead to shift in the characteristic relaxation frequency, $f_c = 1/(2\pi\tau_c)$, toward lower frequencies and to broadening of the relaxation (Levy et al. 2012a). The concept of H-bonded clusters (Fuchs and Kaatze 2001; Ryabov et al. 2001) can account for this phenomena by supposing that a new scale of cooperativity appears, as saccharide concentrations increase, due to the interaction of water clusters with glucose or fructose molecules (Pártay et al. 2007). Naturally, this leads to an overall increase in the characteristic relaxation time for water.

Concentrating only on the $\alpha(\ln\tau)$ plane (see Fig. 10 and the projection YZ in Fig. 11a), the interaction of water with glucose can be analyzed in terms of the formulism described above. The critical derived parameters are $\tau_c \cong 1.3$ ps, $N_{0\tau} = 2.2$. Fructose provided comparable values: $\tau_c \cong 1.2$ ps, $N_{0\tau} = 2.8$ [4]. The cutoff relaxation time $\tau_c \sim 1$ ps is in good agreement with the assumed reorientation time of a single water molecule in the bulk (Barthel et al. 1990; Brovchenko et al. 2004). The number of elemental acts, $N_{0\tau}$, associated with this cutoff time, τ_c, suggests that in the timeframe [0, τ_c], only 2 to 3 relaxation acts, most likely on the level of single water molecules, are involved in the relaxation of the elemental volume. To understand what this "elemental volume" is, we turn to the third, as yet unconsidered, aspect of the relaxation. The coupling between the number density of the relaxation acts N_τ and the molecular structure can be analyzed using the B function (Eq. 7). The macroscopic dipole moment M in Eq. (7) can be considered as the vector sum of all dipole moments, both of the water molecules and of the monosaccharide. It is possible to derive an estimation of the number of water molecules interacting with a single glucose molecule, N_{cl}, when the concentration of glucose is low (a dilute limit) using Eq. (7). This was found to be $N_{cl} \sim 17$–18 water molecules per molecule (Levy et al. 2012a). This is in fair agreement with recent results from molecular dynamic simulation for the first hydration shell of glucose, about 11 water molecules (Caffarena and Grigera 1999; Suzuki 2008).

Simple ionic solutions

The essential difference between a monosaccharide solution and an ionic solution, such as simple salts like NaCl, is in the nature of the interaction with water. For an ionic solution, it is essentially a charge–dipole rather than a dipole–dipole as before. There are numerous studies of the dielectric properties of simple electrolyte solutions (Buchner et al. 1999; Chen et al. 2003; Gulich et al. 2009; Noertemann et al. 1997; Peyman et al. 2007), and it is instructive to see how the 3D trajectory approach compares to them. The results of the 3D trajectory approach, applied to an isothermal, concentration-based microwave dielectric study of diluted NaCl and KCl solutions (Levy et al. 2012b), were presented recently. In contrast to the monosaccharides, the characteristic relaxation frequencies, f_c, shifted toward higher frequencies. In similarity, there was a decrease in the dielectric strength and symmetrical broadening of the main relaxation peak with increasing ionic concentration. The decrease in the characteristic relaxation time, $\tau_c = 1/(2\pi f_c)$, can be attributed to the migration of water molecules from the mesoscopic water cluster to the hydration shell of the solvated ions, leading to a small cluster and a faster relaxation (Levy et al. 2012b). The difference from the nonionic solutions is reflected in 3D trajectory patterns (compare a and b of Fig. 11). This time the function $\alpha(\ln\tau)$ (YZ projection) is in the

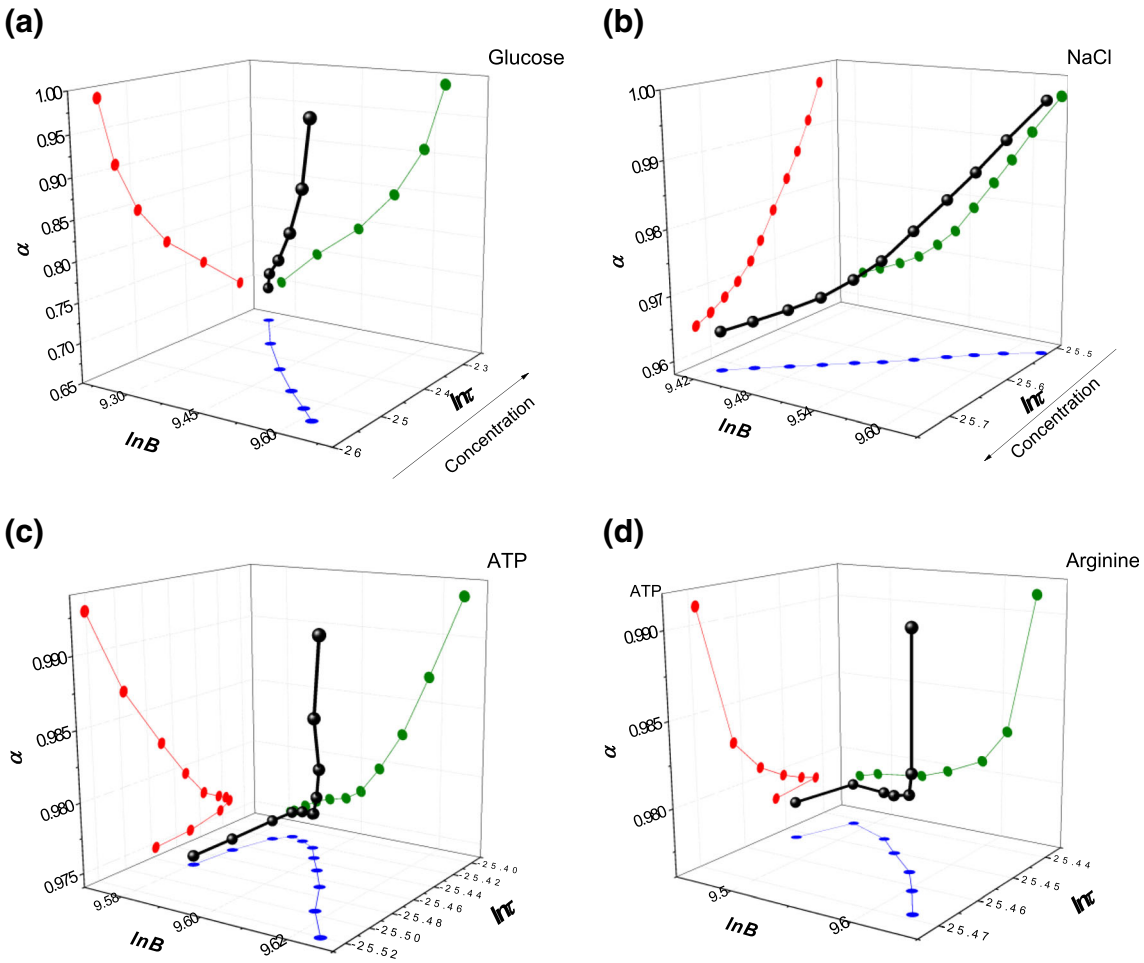

Fig. 11 3D trajectories of CC relaxation processes of different aqueous solutions at 25 °C: **a** glucose, **b** NaCl, **c** ATP, and **d** arginine (reproduced with permission from Copyright 2012, 2014 American Institute of Physics). The vertical axis is α, the stretching parameter defined by Eq. (2); the horizontal axis is the logarithm of the relaxation time, τ, defined by the same Eq. (2); and the logarithm of B, the Froehlich B function, defined in Eq. (7). Together these parameters represent the evolution of the dielectric response of bulk water in these solutions as a function of the change of concentration of the solute. In the case of case of glucose (**a**) and NaCl (**b**), the relaxation times change monotonically with concentration, depending on whether the interaction of the solute with the solvent (water) is dipole–dipole or dipole–ionic, respectively. In the case of biological molecules such as ATP (**c**) and arginine (**d**), the concentration dependence reveals kink points in the dielectric parameters as the dominant behavior varies between dipole–dipole and dipole–ionic

second quadrant of the plane ($\tau < \tau_c$; $\alpha > A$). Using Eqs. (4)–(7), it was found that $\tau_c \cong 8.7$ ps, $N_{0\tau} \cong 1$ for NaCl and $\tau_c \cong 8.5$ ps, $N_{0\tau} \cong 1$ for KCl solutions (Levy et al. 2012b). The value of the cutoff relaxation time τ_c corresponds to relaxation time of the water cluster in bulk water ($c \to 0$) (Barthel et al. 1990; Eisenberg and Kauzmann 1969; Wei et al. 1992) and $N_{0\tau} \sim 1$ implies that the elemental relaxation is that of the water cluster, the natural mesoscopic volume element of water. This contrasts to the case of the dipole–dipole interaction where $\tau_c \sim 1$ ps (Levy et al. 2012a).

A deeper understanding of this fundamental difference comes once one considers the B function of Eq. (7) (Levy et al. 2012b). One can consider the relaxation of dilute ionic solutions as consisting of two subsystems where the first would be the bulk water clusters, shrinking as they lose water to the hydration shells and the second would be the hydration shell–ion core. In the frequency region considered, only the first subsystem is directly visible. Such a representation describes the interactions between all the model components: water dipoles inside the hydration shells, hydration shell/bulk water interface, and the water dipoles in the bulk. In a dilute solution, the interaction of hydration shell to hydration shell can be neglected. With these assumptions in place, one can derive from the experimental dependence of B on the ionic concentration that the average number, N_{av}, of water molecules in a aqueous solution of 0.1 mol/L, perturbed by a single Na^+, Cl^- ion pair would be 33. This drops to $N_{av} = 24$ for a 1-mol/L concentration. At the same concentrations, the corresponding values for the pair K^+, Cl^- are 40 and 22 molecules (Levy et al. 2012b). These values correspond nicely to those found in the literature (Marcus 2014).

Nucleotide and amino acid solutions

Then the same approach has been applied to aqueous solutions of nucleotides (AMP/ATP) and several amino acids (Levy et al. 2014; Puzenko et al. 2012). The dual dipole/charge nature is the main feature of these very important biological molecules. In these cases, both ionic–dipole and dipole–dipole interactions should be present. The dipole moment of amino acids, due to their zwitterionic nature, determines their interaction with the solvent and reflects mostly a dipole–dipole interaction. However, at high concentrations, the strong ionic contribution of nucleotides leads to clear dipole–ion interaction. Not surprisingly, the function $\alpha(\ln\tau)$ (Fig. 11c), driven by solute concentration, reflects this fact. These nucleotides have relatively large dipole moments (~45 D for AMP (Livshits et al. 2009; Meyer-Almes and Porschke 1997) and ~230 D for ATP (Lampinen and Noponen 2005)). One notes an $\alpha(\ln\tau)$ behavior similar to monosaccharides and amino acid solutions (Levy et al. 2012a) for AMP/ATP solutions at low concentrations (less than 3.5%). As expected, the 3D trajectory in Fig. 11c passes a critical concentration point and assumes behavior more reminiscent of ionic solutions with $\alpha(\ln\tau)$ (YZ projection) in the second quadrant of the plane ($\tau < \tau_c$; $\alpha > A$). Accordingly, both AMP and ATP solutions are characterized by two cutoff times τ_c that correspond to different branches of Eq. (5).

At low concentrations (Levy et al. 2012a), the cutoff times τ_c are much longer than 1 ps and close to the relaxation time of the bulk water at the same temperature (~ 8.28 ps at 25 °C; Kaatze 2007). The number of elemental acts in both cases, $N_{0\tau}$, for nucleotides and amino acids is about 1. While this behavior is reminiscent of that noted for ionic solutions, $\tau > \tau_c$, this characterizes the behavior of dipole–dipole interaction. The conclusion is that on this level of cooperativity a relaxation is mediated by a single elemental act of reorientation in the mesocluster (Miyazaki et al. 2008; Puzenko et al. 2012). Above the critical concentration (2nd quadrant, $\tau < \tau_c$, $\alpha > A$), the asymptotic value τ_c approaches the value typical to an ionic solution (Levy et al. 2012b) as their zwitterionic nature leads to stronger ionic contributions. However, τ_c in that case is slightly higher than expected for an ionic solution, indicating yet another cluster dimension for the solvent.

From the behavior of $\alpha(\ln\tau)$ alone, one can deduce the duality of AMP/ATP and amino acid matrixes in terms of water–ion and water–dipole interaction. It is, therefore, natural to ask if this is reinforced by the picture found in the $\ln B(\ln\tau)$ plane. $\ln B(\ln\tau)$ is associated with a dramatic transformation of the mesostructures involved with the relaxation of water as a function of nucleotides' concentration (Puzenko et al. 2012). Using the same formulism to calculate N_{cl}, the number of water molecules directly interacts with the nucleotide. One finds that as the concentration of AMP/ATP changes, N_{cl} decays.

The additional two terminal phosphates in the ATP molecule in comparison with AMP intensifies significantly the transition of water molecules from the bulk state to the hydrated shells as concentrations change (Puzenko et al. 2012). Amino acids, on the other hand, cannot bind so many water molecules and N_{cl} for them does not usually exceed a few dozen. The exception to this rule is for proline (~70 molecules), which has an unusual zwitterionic form (Levy et al. 2014).

The hypothesis for glucose sensitivity—γ dispersion

As a result of the above in vitro measurements, a hypothesis was suggested that during the process of glycolysis in biological cells, the balance between the bulk and bound water is significantly changed. It is to this change that DS is thus sensitive to the effect of glucose concentration changes in the blood. Indeed, it was shown that if every glucose molecule binds ~18 water molecules (Levy et al. 2012a), the ATP molecule can bind up to 140 water molecules (Puzenko et al. 2012). In order to verify this idea, a series of comprehensive studies of RBC suspensions exposed to different glucose concentrations was provided in the microwave frequency range of the main relaxation peak of water (γ process) (Levy et al. 2016). Experimental setup details and results are presented in the following section.

RBC suspensions

Cell preparation

The preparation of red blood cells followed the protocol detailed in Livshits et al. (2009). Three samples of human blood were collected from healthy donors (upon their consent under the Helsinki Ethics Committee (#0568-12-HMO), Hadassah Hospital, Israel). These samples were placed in plastic vacutainers (BD Vacutainer® PST™) with lithium heparin (68 I.U.). Centrifugation was used to isolate RBC. The resulting RBC were washed (twice) from their plasma, again by centrifugation (500×*g* for 10 min) in PBS, and then resuspended at a hematocrit of about 15% in PBS (pH 7.4). The rationale behind this procedure was to preserve the biconcave shape of the cells. The RBC suspension concentration was controlled by a complete blood counter (Automated Hematology Analyzer, XP-300, Symex America, Inc, USA). The washed and isolated erythrocytes were then resuspended in PBS and supplied with nine concentrations of D-glucose (Sigma-Aldrich G5400, 0, 2, 5, 8, 10, 12, 15, 18, and 20 mM). In order to keep the final osmolarity of the suspensions

constant, a corresponding concentration of L-glucose (Sigma-Aldrich G5500) had to be added to the PBS solution for each concentration batch. L-Glucose is an optic enantiomer of D-glucose that is not transportable through the erythrocyte membrane and is frequently used as a control in glucose transport and kinetic studies.

Dielectric spectroscopy

Dielectric measurements were carried out in the frequency range from 500 MHz to 50 GHz using a Vector Network Analyzer (Keysight N5245A PNA-X), together with a Flexible Cable and Slim-Form Probe (Keysight N1501A Dielectric Probe Kit). Three references were used to calibrate the system: air, a Keysight standard short circuit, and pure water at 25 °C. An in-house design for liquids was used to hold the measurement sample. The total volume of the sample was about 7.8 mL. This guaranteed the minimum volume of liquid surrounding the Slim Form Probe to ensure a reliable dielectric measurement. The holder was enveloped by a thermal jacket and attached to a Julabo CF 41 oil-based heat circulatory system. The cell was held at 25 ± 0.1 °C. The measurement room was air-conditioned and maintained at 25 ± 1 °C. Each sample was measured at least six times. The real and imaginary parts $\varepsilon'(\omega)$ and $\varepsilon''(\omega)$ were evaluated using the Keysight N1500A Materials Measurement Software with an accuracy of $\Delta\varepsilon'/\varepsilon' = 0.05$, $\Delta\varepsilon''/\varepsilon'' = 0.05$ (Keysight 2012).

When D-glucose was added to PBS, the cells were first incubated for 5 min at 25 °C before measurements.

Determination of RBC deformability

The physical properties of RBC were characterized by a computerized cell flow-properties analyzer (CFA), designed and constructed in-house (Relevy et al. 2008). The CFA monitors the hemodynamic characteristics of RBC as a function of shear stress, under conditions resembling those in microvessels. The dynamic organization of the cells is monitored in a narrow-gap flow chamber by a microscope (Barshtein et al. 2014; Chen et al. 1995; Relevy et al. 2008). RBC deformability is determined by measuring the elongation of RBC, while they are stuck to a polystyrene slide, under flow-induced sheer stress (Relevy et al. 2008); 50 μL of RBC suspension (1% hematocrit, in PBS) is allowed into the flow chamber (adjusted to 200 μm gap) that contains an uncoated slide (purchased from Electron Microscopy Science, Washington, PA). The RBC that adhere to the slide surface are then subjected to controllable flow-induced sheer stress (3.0 Pa). Deformity is expressed by the elongation ratio: ER = a/b, where a is the major cellular axis and b is the minor cellular axis. ER = 1 reflects a round RBC. The process is automated and an image analysis program automatically calculates ER. The deformability distribution of the RBC population (at least 2500 ± 300 cells) is then provided as a function of shear stress (Relevy et al. 2008). The measurement accuracy of the axes is about 10%. RBC with ER ≤ 1.1 are defined as "undeformable" cells.

Dielectric spectra of cytoplasm

Fig. 12a shows a typical example of the dielectric losses for a RBC suspension at 25 °C. As a comparison, the black line shows the losses of pure water. For clarity, dc conductivity has been removed from both spectra.

At these frequencies, there is no impact to the dielectric losses from the plasma membrane of the cell. As the contributing factors here are of the cytoplasm and the PBS suspension, one can obtain the relative permittivity of the cytoplasm by using an appropriate mixture equation (Asami 2015; Ermolina et al. 2001). The optimal model in this case was first presented by Kraszewski et al. (1976), who considered microwave propagation in a heterogeneous medium. This model assumes that a biphasic suspension can be considered as a sum of an infinite number of thin water and substance layers, each of thickness $\delta t \ll \lambda$, where λ is the free-space wavelength. The resulting formula isolates the permittivity of the cellular interior by:

$$\varepsilon^*_{\text{cell}} = \left(\frac{(\varepsilon^*_{\text{mix}})^{1/2} - (\varepsilon^*_{\text{buff}})^{1/2}(1-\varphi)}{\varphi} \right)^2 \tag{8}$$

Here, $\varepsilon^*_{\text{mix}}$, $\varepsilon^*_{\text{cell}}$, and $\varepsilon^*_{\text{buff}}$ are the dielectric permittivity of the mixture, the interior of the cell, and the buffer, respectively. The volume fraction of the RBC (hematocrit) is represented by φ. Using this formulism, Fig. 12b shows the loss spectra of the cytoplasm for two different glucose concentrations.

The recalculated spectra were fitted using an in-house software, Datama (Axelrod et al. 2004), capable of simultaneously modeling both the real and imaginary components of the measured permittivity. The spectra were fitted to the CC function (Eq. 2) and the results are shown by the solid lines in Fig. 12b. The relaxation times of the cytoplasm are presented in Fig. 13a. The notable feature is the decrease of the relaxation times as the concentration of D-glucose increases, until reaching a critical concentration (10 mM), after which the trend is reversed. It is reminiscent of the D-glucose concentration behavior of the β dispersion of spherical RBC noted by Hayashi et al. (2003). When glucose uptake by the cell begins, there is an influx of water, which impinges on electrolyte distribution of the cell interior: firstly causing electrolyte dilution in submembrane and cytosolic compartments and further activating ion-dependent processes in

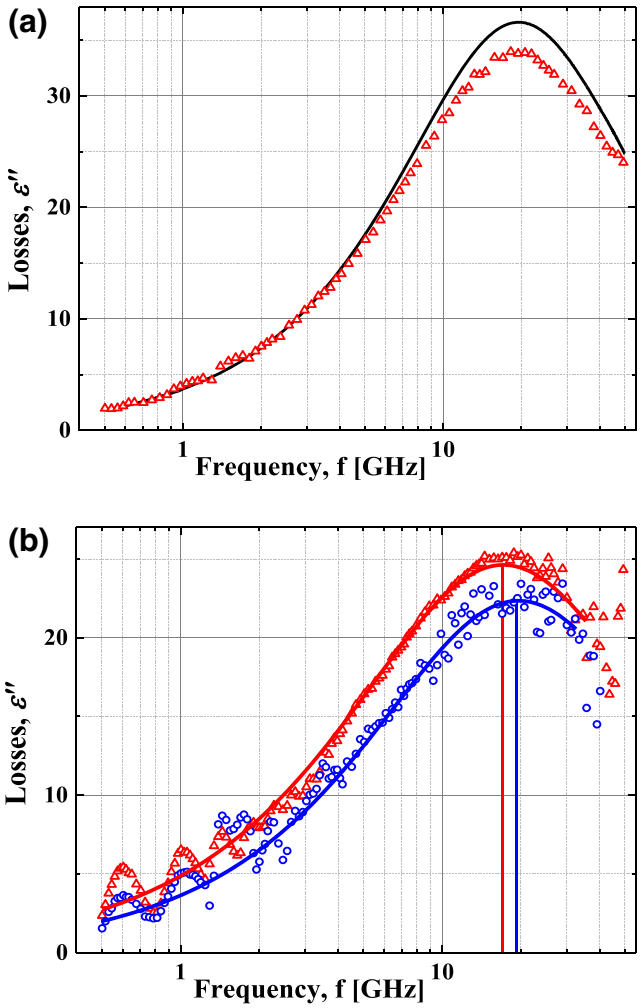

Fig. 12 In panel **a** are shown the dielectric loss spectra at 25 °C of an RBC suspension in PBS (red triangles) compared to water (black line). Dc conductivity has been removed. In panel **b** are shown the derived losses of cellular cytoplasm without D-glucose (red triangles) and 10 mM D-glucose (blue circles). The lines are the fitting curves (reproduced with permission from Copyright 2016, American Chemical Society)

order to release water excess (Fischbarg et al. 1990; Iserovich et al. 2002; Lang et al. 1998). Furthermore, glucose utilization leads to charged glycolytic metabolites (such as ATP) and further related electrolyte reorganization (Caduff et al. 2011; Fischbarg et al. 1990; Hillier et al. 1999; Jiang et al. 2006; Kang 2015; Mercer and Dunham 1981). Using the formulism of $\alpha(\ln\tau)$, derived from the fitting to Eq. (2) and outlined in the "Theoretical background" section, one can gain insight to the processes happening during glucose uptake. The results are plotted in Fig. 13b. The curvature of the $\alpha(\ln\tau)$ dependence for $c < 10$ mM is indicative of a dipole–ion interaction—an expected result, given the consequences of glycolysis (Livshits 2007; Raicu and Feldman 2015). The elementary relaxation cutoff time, τ_c, is equal to 10.1 ps, significantly higher than the typical characteristic relaxation time for water at the same temperature. As noted above in the "Theoretical background" section, purely ionic solutions at the same temperature usually have τ_c on par with the relaxation time of bulk water (Levy et al. 2012b; Puzenko et al. 2012). This discrepancy between τ_c in pure solutions and that of the cytoplasm hints at new structures of water, not quite those of traditional bulk water and not those of the traditional hydration shell. Something similar was proposed and observed by the group of Havenith (Ebbinghaus et al. 2007; Grossman et al. 2011; Heugen et al. 2006; Heyden et al. 2010) in their investigation of the hydration shells in electrolyte solutions using terahertz spectroscopy. Additionally, N_0, the density of relaxation acts during τ_c, tends toward 1, akin to the situation in ionic aqueous solutions. However, in our case, the values of τ_c are closer to those found in high concentrations (0–130 and 0–93 mmol/L, respectively) of AMP/ATP in solution (Puzenko et al. 2012). With over 300,000 GLUT1 transporters per cell (a concentration of $N = 10^{24}$ m^{-3}) and up to 200 water molecules participating in the hydration shell of ATP, our conclusion is that during glycolysis, the dominant factor regulating the relaxation of these water structures is the exchange of a water molecule with the hydration shells around ATP (Livshits et al. 2009).

However, the story is upended once D-glucose concentrations approach 10–12 mM. Now the GLUT1 transporter "closes" by the action of ATP (Livshits et al. 2009), in order to protect the cell from an abundance of glucose. ATP molecules concentrate near the membrane and interact with the GLUT1 transporters (Livshits et al. 2009). They effectively regulate the transport activity. While buffer D-glucose concentrations increase outside the cell, osmotic pressure is maintained by an influx of extracellular Na^+ and an efflux of intracellular K^+ (Caduff et al. 2011; Hillier et al. 1999). Concurrently, the relaxation times increase with increasing concentration and the dependencies of $\alpha(\ln\tau)$ move to the first quadrant of the hyperbole scheme of $\alpha(\ln\tau)$ (see Fig. 10). The fitting parameters are τ_c equal to 7.42 ps and N_0 still tends toward 1 (Levy et al. 2016). It is tempting to think that the relaxation becomes dominated by a dipole–dipole interaction. However, such a direct analogy to monosaccharide solutions (Levy et al. 2012a) would be too simplistic. As the relaxation times are in proportion to the size of water structures, this indicates a change in the effective length scales that dictate these water structures. Possibly, this suggests that in the competition for water between ATP–GLUT1 complexes in the membrane and incoming Na^+, water moves back toward the cellular interior.

The concurrent B function, shown in Fig. 14, monotonically decays with increasing of D-glucose concentrations. There could be a number of explanations: (1) with the process of glycolysis, water is increasingly solvated in hydration shells of ATP (Puzenko et al. 2012), leaving fewer defined water structures in the cellular interior; or (2) it could also point to

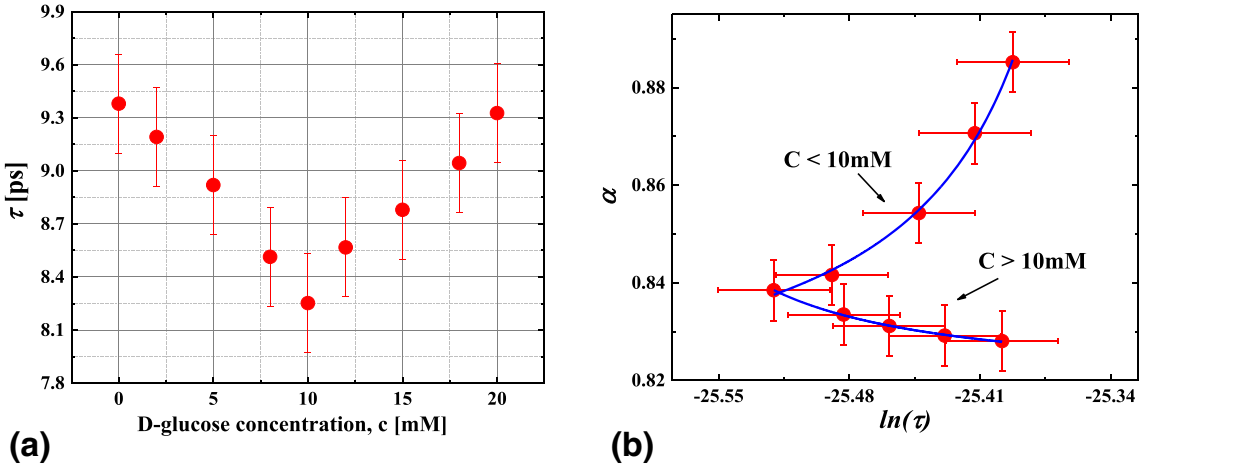

Fig. 13 In panel **a** are shown the experimental relaxation times of cytoplasmic water for one cell in the presence of varying buffer concentrations of D-glucose. In panel **b**, $\alpha(\ln\tau)$ is shown dependence for one cell at 25 °C. Solid lines are the fitting curves using Eq. (6) (Levy et al. 2016) (reproduced with permission from Copyright 2016, American Chemical Society)

the struggle by the cell to maintain its integrity as glucose intake increases, by a reorganization of interior water structures. This conflict becomes obvious in the concentration behavior of the elongation ratio (see Fig.15).

Fig. 15 shows that the elongation ratio peaks at same concentration point as that of the minimum of the cytoplasm relaxation times (10–12 mM). The deformability of RBC is regulated by several interrelated mechanisms. They involve numerous membrane and cytosolic proteins, such as spectrin also being the main protein forming the membrane skeleton.

As reported by Johnson et al. (2007) and later by Manno et al. (2010), and similar with the regulation of membrane flexibility under sheer forces, the cytoskeleton undergoes conformational changes with the increasing glucose concentration and its metabolic processing that forces the RBC to modify the structure. It will need to be further investigated how that can be linked with the basic phenomena shown on the glucose-induced ATP production and, consequently, its effect on the dielectric characteristics via its impact on water.

Here, it is postulated that these structural processes are directly and indirectly affected by glucose and so should also be influenced by the action of ATP on the GLUT1 transporters at the critical concentration (Livshits et al. 2009; Mohandas and Gallagher 2008). This remains to be further investigated.

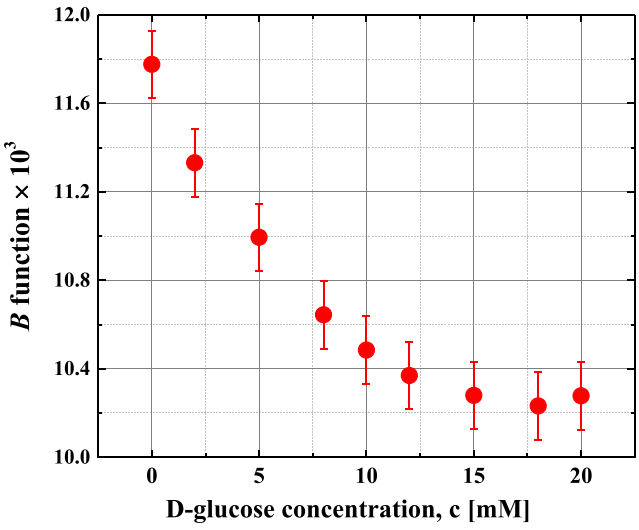

Fig. 14 The D-glucose concentration dependence of the *B* function (Levy et al. 2016) as defined by Eq. (7), of the cytoplasmic water relaxation for the red blood cell (reproduced with permission from Copyright 2016, American Chemical Society)

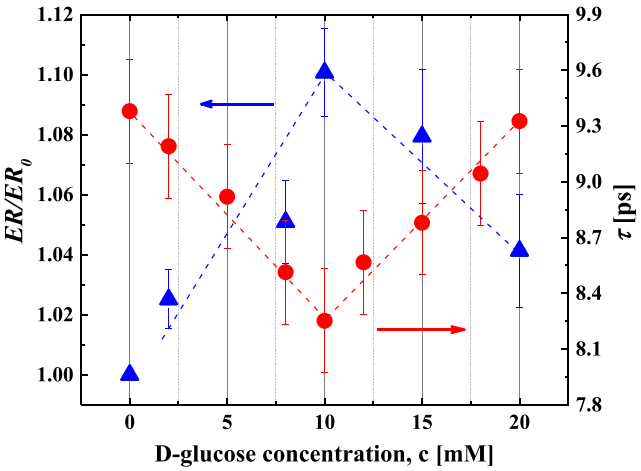

Fig. 15 The elongation ratio of red blood cells in the presence of varying concentrations of D-glucose (blue triangles).The red dots are the relaxation times of the main peak of cytoplasmic water (Levy et al. 2016) for the same concentrations. The critical point, 10 mM, is represented in both data sets and indicates the cessation of glucose uptake by the cell because of the formation of ATP–GLUT1 complexes, effectively blocking the GLUT1 transporter (reproduced with permission from Copyright 2016, American Chemical Society)

Conclusions

In conclusion, one must first note that in an in vivo situation, glucose metabolism is a sophisticated cascade of biochemical reactions, taking place in a complex 3D multicompartment system with different permeabilities and overlaying dynamics. These processes take place over several tissue/vascular compartments, resulting in a hierarchy of time scales and products, including the distribution of free and bound water as well as redistribution of electrolytes. Consequently, NIGM has been drawn inexorably toward multisensory platforms that can address the perturbations characterizing the underlying biophysical mechanisms.

However, the above results demonstrate the connection of the cytoplasm water to functionality as reflected by the membrane integrity of RBC. While the cascade of biochemical reactions is complex, the dielectric response of water is straightforward and governed by the final product of glycolysis.

As such, it can act as an efficient marker responding to glucose exposure. One would hope that this further evolved understanding of this mechanistic contribution could also provide a further advanced vista on noninvasive glucose monitoring.

Extensive experimental in vitro and in vivo experiences and published evidence have been collected that will continue to help further solidify the current understanding. For the next phase, we are seeing a number of experiments to be of interest. These are namely (a) selectively blocking GLUT1 and GLUT5 in RBC and then exposing the cells to both glucose and fructose as well as to other carbohydrates (one would expect that this should yield comparable results to those obtained when RBC are exposed to nonmetabolized L-glucose); (b) continuation of the investigation into the relationship between glucose, glycolysis, resulting ATP, and behavior of the membrane; and (c) continuation of the investigation of hosts exposed to glucose studied in the γ dispersion to further validate the causality of ATP and membrane interactions.

References

Abe K, Niikura Y, Fujimoto T, Akaishi T, Misawa M (2008) Involvement of dopamine D2 receptors in the induction of long-term potentiation in the basolateral amygdala-dentate gyrus pathway of anesthetized rats. Neuropharmacology 55:1419–1424

Agmon N (1996) Tetrahedral displacement: the mechanism behind the Debye relaxation in water. J Phys Chem 100:1072–1080

Aguirre A, Testa-Weintraub LA, Banderas JA, Haraszthy GG, Reddy MS, Levine MJ (1993) Sialochemistry: a diagnostic tool? Crit Rev Oral Biol Med 4:343–350

Asami K (2002a) Characterization of biological cells by dielectric spectroscopy. J Non-Cryst Solids 305:268–277

Asami K (2002b) Characterization of heterogeneous systems by dielectric spectroscopy. Prog Polym Sci 67:1617–1659

Asami K (2014) Low-frequency dielectric dispersion of bacterial cell suspensions. Colloids Surf B Biointerfaces 119:1–5

Asami K (2015) Radiofrequency dielectric properties of cell suspensions. In: Raicu V, Feldman Y (eds) Dielectric relaxation in biological systems: physical principles, methods, and applications. Oxford University Press, Oxford, pp 340–362

Asami K, Yonezawa T (1995) Dielectric analysis of yeast cell growth. Biochim Biophys Acta 1245:99–105

Ascaso FJ, Huerva V (2016) Noninvasive continuous monitoring of tear glucose using glucose-sensing contact lenses. Optometry Vision Sci 93:426–434

Axelrod N, Axelrod E, Gutina A, Puzenko A, Ben Ishai P, Feldman Y (2004) Dielectric spectroscopy data treatment: I. Frequency domain. Meas Sci Technol 15:755–764

Bagchi B (2012) From anomalies in neat liquid to structure, dynamics and function in the biological world. Chem Phys Lett 529:1–9

Barshtein G, Gural A, Manny N, Zelig O, Yedgar S, Arbell D (2014) Storage-induced damage to red blood cell mechanical properties can be only partially reversed by rejuvenation. Transfus Med Hemoth 41:197–204

Barthel J, Bachhuber K, Buchner R, Hetzenauer H (1990) Dielectric spectra of some common solvents in the microwave region. Water and lower alcohols. Chem Phys Lett 165:369–373

Ben Ishai P, Tripathi SR, Kawasa K, Puzenko A, Feldman Y (2015) What is the primary mover of water dynamics? PCCP 17:15428–15434

Beving H, Eriksson LEG, Davey CL, Kell DB (1994) Dielectric properties of human blood and erythrocytes at radio frequencies (0.2-10 MHz); dependence on cell volume fraction and medium composition. Eur Biophys J 23:207–215

Brovchenko I, Geiger A, Oleinikova A (2004) Clustering of water molecules in aqueous solutions: effect of water–solute interaction. Phys Chem Chem Phys 6:1982–1987

Brownlee M (2005) The pathobiology of diabetic complications: a unifying mechanism. Diabetes 54:1615–1625

Buchner R, Hefter GT, May PM (1999) Dielectric relaxation of aqueous NaCl solutions. J Phys Chem A 103:1–9

Caduff A (2004) Non-invasive RF system for glucose monitoring, vol Doctor of Philosophy. University of Teesside

Caduff A, Talary M (2015) Glucose detection from skin dielectric measurement. In: Raicu V, Feldman Y (eds) Dielectric relaxation in biological systems. Oxford University Press, Oxford, pp 388–412

Caduff A, Hirt E, Feldman Y, Ali Z, Heinemann L (2003a) First human experiments with a novel non-invasive, non-optical continuous glucose monitoring system. Biosens Bioelectron 19:209–217

Caduff A, Hirt E, Feldman Y, Heinemann L (2003b) First human trials with a novel non-invasive, non-optical continuous glucose monitoring system. Biosens Bioelectron 19:209–217

Caduff A, Dewarrat F, Talary MS, Stalder G, Heinemann G, Feldman Y (2006) Non-invasive glucose monitoring in patients with diabetes: a novel system based on impedance spectroscopy. Biosens Bioelectron 22:598–604

Caduff A, Talary MS, Zakharov P (2010) Cutaneous blood perfusion as a perturbing factor for noninvasive glucose monitoring. Diabetes Technol Ther 12:1–9

Caduff A, Lutz HU, Heinemann L, Benedetto GD, Talary MS, Theander S (2011) Dynamics of blood electrolytes in repeated hyper- and/or hypoglycaemic events in patients with type 1 diabetes. Diabetologia 54:2678–2689

Caduff A, Zanon M, Mueller M, Zakharov P, Feldman Y, Feo OD, Donath M, Stahel WA, Talary MS (2015) The effect of a global, subject, and device-specific model on a noninvasive glucose monitoring multisensor system. J Diabetes Sci Technol 9:865–872

Caduff A, Zanon M, Zakharov P, Mueller M, Talary M, Krebs A, Stahel WA, Donath M (2018) First experiences with a wearable

multisensor in an outpatient glucose monitoring study, part I: the users' view. J Diabetes Sci Technol 12:562–568
Caffarena ER, Grigera JR (1999) Hydration of glucose in the rubbery and glassy states studied by molecular dynamics simulation. Carbohydr Res 315:63–69
Chaplin M (2000) A proposal for the structuring of water. Biophys Chem 83:211–221
Chen S, Gavish B, Zhang S, Mahler Y, Yedgar S (1995) Monitoring of erythrocyte aggregate morphology under flow by computerized image analysis. Biorheology 32:487–496
Chen T, Hefter G, Buchner R (2003) Dielectric spectroscopy of aqueous solutions of KCl and CsCl. J Phys Chem A 107:4025–4031
Choi H, Nylon J, Luzio S, Beutler J, Porch A (2015) Design of continuous non-invasive blood glucose monitoring sensor based on a microwave split ring resonator. IEEE Trans Microwave Theory Tech 63:3016–3025
Chowdhury MK, Srivastava A, Sharma N, Sharma S (2016) Noninvasive blood glucose measurement utilizing a newly designed system based on modulated ultrasound and infrared light. Int J Diabetes Dev Countries 36:439–448
Coffey WT (2004) Dielectric relaxation: an overview. J Mol Liq 114:5–25
Coffey WT, Kalmykov YP, Titov SV (2006) Fractional rotational diffusion and anomalous dielectric relaxation in dipole systems. In: Coffey WT, Kalmykov YP (eds) Advances in chemical physics, vol 133, New York, p 285
Cole KS, Cole RH (1941) Dispersion and absorption in dielectrics I. Alternating current characteristics. J Chem Phys Eng Data 9:341–351
Danne T, Nimri R, Battelino T, Bergenstal RM, Close KL, DeVries JH, Garg S, Heinemann L, Hirsch I, Amiel SA, Beck R, Bosi E, Buckingham B, Cobelli C, Dassau E, Doyle FJ 3rd, Heller S, Hovorka R, Jia W, Jones T, Kordonouri O, Kovatchev B, Kowalski A, Laffel L, Maahs D, Murphy HR, Nørgaard K, Parkin CG, Renard E, Saboo B, Scharf M, Tamborlane WV, Weinzimer SA, Phillip M (2017) International consensus on use of continuous glucose monitoring. Diabetes Care 40:1631–1640
Debye P (1929) Polar molecules. Dover, New York
Dewarrat F, Falco L, Mueller M, Reinhard S, Caduff A, Talary MS (2011) A dielectric inverse problem applied to human skin measurements during glucose excursions. Physiol Meas 32:1285–1300
Ebbinghaus S, Kim SJ, Heyden M, Yu X, Heugen U, Gruebele M, Leitner DM, Havenith M (2007) An extended dynamical solvation shell around proteins. Proc Natl Acad Sci USA 104:20749–20752
Eisenberg D, Kauzmann W (1969) The structure and properties of water. Clarendon, Oxford
Ellison WJ, Lamkaouchi K, Moreau JM (1996) Water: a dielectric reference. J Mol Liq 68:171–279
Ermolina I, Polevaya Y, Feldman Y, Ginzburg BZ, Schlesinger M (2001) Study of normal and malignant white blood cells by time domain dielectric spectroscopy. IEEE Trans Dielectrics Electric Insul 8:253–261
Feldman Y, Ermolina I, Hayashi Y (2003) Time domain dielectric spectroscopy study of biological systems. IEEE Trans Dielectrics E 10:728–775
Feldman Y, Puzenko A, Ryabov Y (2006a) Dielectric relaxation phenomena in complex materials fractals, diffusion, and relaxation in disordered complex systems. Wiley, pp 1-125
Feldman Y, Puzenko A, Ryabov Y (2006b) In advances in chemical physics, part A, fractals, diffusion and relaxation in disordered complex systems. Wiley, New York
Feldman Y, Puzenko A, Ishai PB, Levy E (2013) Dielectric relaxation of water in complex system. In: Kalmykov YP (ed) Recent advances in broadband dielectric spectroscopy; NATO science for peace and security series B: Physics and Biophysics. Springer, Perpignan, pp 1–18
Feldman Y, Puzenko A, Ben Ishai P, Gutina (Greenbaum) A (2014) The dielectric response of interfacial water—from the ordered structures to the single hydrated shell. Colloid Polym 29:1923-1932
Fischbarg J, Kuang KY, Vera JC, Arant S, Silverstein SC, Loike J, Rosen OM (1990) Glucose transporters serve as water channels. Proc Natl Acad Sci U S A 87:3244–3247
Forst T, Caduff A, Talary M, Weder M, Brändle M, Kann P, Flacke F, Ch F, Pfützner A (2006) Impact of environmental temperature on skin thickness and microvascular blood flow in diabetic and non-diabetic subjects. Diabetes Technol Ther 8:94–101
Fröhlich H (1958) Theory of dielectrics; dielectric constant and dielectric loss, 2nd edn. Clarendon, Oxford
Fuchs K, Kaatze U (2001) Molecular dynamics of carbohydrate aqueous solutions. Dielectric relaxation as a function of glucose and fructose concentration. J Phys Chem B 105:2036–2042
Gabriel C, Gabriel S, Corthout E (1996) The dielectric properties of biological tissues: I. Literature survey. Phys Med Biol 41:2231–2249
Garg SK, Akturk HK (2018) A new era in continuous glucose monitoring: Food and Drug Administration creates a new category of factory-calibrated nonadjunctive, interoperable class II medical devices. Diabetes Technol Ther 20:391–394
Grant EH, Sheppard RJ, South GP (1978) Dielectric behaviour of biological molecules in solution. Clarendon Press, Oxford
Grossman M, Born B, Heyden M, Tworowski D, Fields GB, Sagi I, Havenith M (2011) Correlated structural kinetics and retarded solvent dynamics at the metalloprotease active site. Na Struct Mol Biol 18:1102–1113
Guarin G, Hofmann M, Weigel R, Fischer G, Kissinger D (2013) Determination of sugar concentration in aqueous solutions using ultra-wideband microwave impedance spectroscopy Microwave Symposium Digest (IMS), 2013 IEEE MTT-S International. IEEE, Seattl
Gulich R, Köhler M, Lunkenheimer P, Loidl A (2009) Dielectric spectroscopy on aqueous electrolytic solutions. Radiati Environ Biophys 48:107–114
Hayashi Y, Shinyashiki N, Yagihara S (2002) Dynamical structure of water around biopolymers investigated by microwave dielectric measurements using time domain reflectometry method. J Non-Cryst Solids 305:328–332
Hayashi Y, Livshits L, Caduff A, Feldman Y (2003) Dielectric spectroscopy study of specific glucose influence on human erythrocyte membranes. J Phys D: Appl Phys 36:369–374
Hayashi Y, Oshige I, Katsumoto Y, Omori S, Yasuda A, Asami K (2008) Dielectric inspection of erythrocyte morphology. Phys Med Biol 53:2553–2564
Heard K, Fidyk N, Carruthers A (2000) ATP-dependent substrate occlusion by the human erythrocyte sugar transporter. Biochemistry 39:3005–3014
Heugen U, Schwaab G, Bründermann E, Heyden M, Yu X, Leitner DM, Havenith M (2006) Solute-induced retardation of water dynamics probed directly by THz spectroscopy. Proc Natl Acad Sci USA 103:12301–12306
Heyden M, Sun J, Funkner S, Mathias G, Forbert H, Havenith M, Marx D (2010) Dissecting the THz spectrum of liquid water from first principles via correlations in time and space. Proc Natl Acad Sci USA 107:12068–12073
Hilfer R (2000) Fractional time evolution. In: Hilfer R (ed) Applications of fractional calculus in physics. World Scientific, Singapore, pp 87–130
Hillier TA, Abbott RD, Barrett EJ (1999) Hyponatremia: evaluating the correction factor for hyperglycemia. Am J Med 106:399–403
Huang SY, Omkar YY, Inda AJG, Xavier CX, Mu WC, Meng YS (2019) Microstrip line-based glucose sensor for noninvasive continuous monitoring using the main field for sensing and multivariable crosschecking. IEEE Sens J 19:535–547

Iserovich P, Wang D, Ma L, Yang H, Zuniga FA, Pascual JM, Kuang K, De Vivo DC (2002) Fischbarg J. Changes in glucose transport and water permeability resulting from the T310I pathogenic mutation in Glut1 are consistent with two transport channels per monomer. J Biol Chem 277:30991–30997

Jiang W, Ding Y, Su Y, Jiang M, Hu X, Zhang Z (2006) Interaction of glucose transporter 1 with anion exchanger 1 in vitro. Biochem Biophys Res Commun 339:1255–1261

Jintao X, Liming Y, Yufei L, Chunyan L, Han C (2017) Noninvasive and fast measurement of blood glucose in vivo by near infrared (NIR) spectroscopy. Spectrochim Acta A Mol Biomol Spectrosc 179:250–254

Johnson CP, Tang HY, Carag C, Speicher DW, Discher DE (2007) Forced unfolding of proteins within cells. Science 317:663–666

Kaatze U (1989) Complex permittivity of water as a function of frequency and temperature. J Chem Phys Eng Data 34:371–374

Kaatze U (1990) On the existence of bound water in biological-systems as probed by dielectric-spectroscopy. Phys Med Biol 35:1663–1681

Kaatze U (2007) Reference liquids for the calibration of dielectric sensors and measurement instruments. Meas Sci Technol 18:967–976

Kaatze U (2015) Dielectric relaxation of water. In: Raicu V, Feldman Y (eds) Dielectric relaxation in biological systems. Oxford University Press, Oxford, pp 189–278

Kang MY (2015) Blood electrolyte disturbances during severe hypoglycemia in Korean patients with type 2 diabetes. Korean J Intern Med 30:648–656

Keysight (2012) 85070E dielectric probe kit 200 MHz to 50 GHz. Technical overview. Agilent Technologies, Santa Clara

Kraszewski A, Kulinski S, Matuszewski M (1976) Dielectric properties and a model of biphase water suspension at 9.4 GHz. JApplPhys 47: 1275–1277

Kremer F, Schonhals A (2003) Broadband dielectric spectroscopy. Springer, Berlin

Kuang W, Nelson SO (1998) Low-frequency dielectric properties of biological tissues: a review with some new insights. Trans ASAE 41: 173–184

Lampinen MJ, Noponen T (2005) Electric dipole theory and thermodynamics of actomyosin molecular motor in muscle contraction. Theor Biol 236:397–421

Lang F, Busch GL, Ritter M, Voelkl H, Waldegger S, Gulbins E, Haeussinger D (1998) Functional significance of cell volume regulatory mechanisms. Physiol Rev 78:247–306

Lee SJ, Yoon HS, Xuan X, Park JY, Paik S-J, Allen MG (2016) A patch type non-enzymatic biosensor based on 3D SUS micro-needle electrode array for minimally invasive continuous glucose monitoring. Sens Actuat B Chem 222:1144–1151

Levy E, Puzenko A, Kaatze U, Ben Ishai P, Feldman Y (2012a) Dielectric spectra broadening as the signature of dipole-matrix interaction I. Water in nonionic solutions. J Chem Phys 136:114502–114505

Levy E, Puzenko A, Kaatze U, Ishai PB, Feldman Y (2012b) Dielectric spectra broadening as the signature of dipole-matrix interaction II. Water in ionic solutions. J Chem Phys 136:114503–114506

Levy E, Silvina C, Ermolina I, Puzenko A, Feldman Y (2014) Dielectric spectra broadening as a signature for dipole-matrix interaction. IV. Water in amino acids solutions. J Chem Phys 140:135104-135101-135106

Levy E, Barshtein G, Livshitz L, Ishai PB, Feldman Y (2016) The vitality of human RBC and its connection to cytoplasmic water: I The glucose concentration influence. J Phys Chem B 120:10214–10220

Lilienfeld-Toal HV, Weidenmu M, Xhelaj A, Maentele W (2005) A novel approach to non-invasive glucose measurement by mid-infrared spectroscopy: the combination of quantum cascade lasers (QCL) and photoacoustic detection. Vib Spectrosc 38:209–215

Livshits L (2007) Sugar-induced membrane dielectric response in human erythrocytes, vol Doctor of Philosophy. The Hebrew University of Jerusalem

Livshits L, Caduff A, Talary MS, Feldman Y (2007) Dielectric response of biconcave erythrocyte membranes to D- and L-glucose. J Phys D: Appli Phys 40:15-19

Livshits L, Caduff A, Talary MS, Lutz HU, Hayashi Y, Puzenko A, Shendrik A, Feldman Y (2009) The role of GLUT1 in the sugar-induced dielectric response of human erythrocytes. J Phys Chem B 113:2212–2220

Manno S, Mohandas N, Takakuwa Y (2010) ATP-dependent mechanism protects spectrin against glycation in human erythrocytes. J Biol Chem 285:33923–33929

Marcus Y (2014) Concentration dependence of ionic hydration numbers. J Phys Chem B 118:10471–10476

Mensing C, Boucher J, Cypress M, Weinger K, Mulcahy K, Barta P, Hosey G, Kopher W, Lasichak A, Lamb B, Mangan M, Norman J, Tanja J, Yauk L, Wisdom K, Adams C (2004) The Expert Committee on the diagnosis and classification of diabetes mellitus. Diabetes Care 27:s5–s10

Mercer RW, Dunham PB (1981) Membrane-bound ATP fuels the Na/K pump. Studies on membrane-bound glycolytic enzymes on inside-out vesicles from human red cell membranes. J Gen Physiol 78:547–568

Metzler R, Klafter J (2000) The random walk's guide to anomalous diffusion: a fractional dynamics approach. Physics Reports 339:1–77

Meyer-Almes FJ, Porschke DJ (1997) The cyclic AMP receptor promoter DNA complex: a comparison of crystal and solution structure by quantitative molecular electrooptics. Mol Biol 269:842–850

Miyazaki T, Mogami G, Wazawa T, Kodama T, Suzuki M (2008) Measurement of the dielectric relaxation property of water-ion loose complex in aqueous solutions of salt at low concentrations. J Phys Chem A 112:10801–10806

Mohandas N, Gallagher PG (2008) Red cell membrane: past, present, and future. Blood 112:3939–3948

Nathan DM (2014) The diabetes control and complications trial/epidemiology of diabetes interventions and complications study at 30 years: overview. Diabetes Care 37:9–16

Nikawa Y, Someya D (2001) Non-invasive measurements of blood sugar level by millimeter waves 2001 IEEE MTT-S International Microwave Sympsoium Digest (Cat No01CH37157), Phoenix.

Noertemann K, Hilland J, Kaatze U (1997) Dielectric properties of aqueous NaCl solutions at microwave frequencies. J Phys Chem A 101: 6864–6869

Oleinikova A, Brovchenko I, Geiger A, Guillot B (2002) Percolation of water in aqueous solution and liquid-liquid immiscibility. J Chem Phys Eng Data 117:3296–3304

Pártay LB, Jedlovszky P, Brovchenko I, Oleinikova A (2007) Formation of mesoscopic water networks in aqueous systems. Phys Chem Chem Phys 9:1341–1346

Pethig RR (1977) In: Davies M (ed) Dielectric and related molecular processes, vol 3. London, The Chemical Society

Pethig RR (1979) Dielectric and electronic properties of biological materials. Wiley, Chichester

Pethig RR, Kell DB (1987) The passive electrical properties of biological systems: their significance in physiology, biophysics and biotechnology. Phys Med Biol 32:933–970

Peyman A, Gabriel C, Grant EH (2007) Complex permittivity of sodium chloride solutions at microwave frequencies. Bioelectromagnetics 28:264–274

Pfutzner A, Caduff A, Larbig M, Schrepfer T, Forst T (2004) Impact of posture and fixation technique on impedance spectroscopy used for continuous and noninvasive glucose monitoring. Diabetes Technol Ther 6:435–441

Popov I, Ishai PB, Khamzin A, Feldman Y (2016) The mechanism of the dielectric relaxation in water. Phys Chem Chem Phys 18:13941–13953

Puzenko A, Ishai PB, Feldman Y (2010) Cole-Cole broadening in dielectric relaxation and strange kinetics. Phys Rev Lett 105:037601–037604

Puzenko A, Levy E, Shendrik A, Talary MS, Caduff A, Feldman Y (2012) Dielectric spectra broadening as a signature for dipole-matrix interaction. III. Water in adenosine monophosphate/adenosine-5′-triphosphate solutions. J Chem Phys 137:194502–194508

Raicu V, Feldman Y (2015) Dielectric relaxation in biological systems: physical principles, methods, and applications. Oxford University Press, Oxford

Relevy H, Koshkaryev A, Manny N, Yedgar S, Barshtein G (2008) Blood banking-induced alteration of red blood cell flow properties. Transfusion 48:136–146

Ribet F, Stemme G, Roxhed N (2017) Ultra-miniaturization of a planar amperometric sensor targeting continuous intradermal glucose monitoring. Biosens Bioelectron 90:577–583

Rodbard D (2016) Continuous glucose monitoring: a review of successes, challenges, and opportunities. Diabetes Technol Ther 18:S2-3-S2-13

Rodríguez-Arteche I, Cerveny S, Alegría A, Colmenero J (2012) Dielectric spectroscopy in the GHz region on fully hydrated zwitterionic amino acids Phys Chem Chem Phys:11352-11362

Ryabov Y, Gutina A, Arkhipov V, Feldman Y (2001) Dielectric relaxation phenomena of water absorbed in porous glasses. J Phys Chem B 105:1845–1850

Ryabov YE, Feldman Y, Shinyashiki N, Yagihara S (2002) The symmetric broadening of the water relaxation peak in polymer–water mixtures and its relationship to the hydrophilic and hydrophobic properties of polymers. J Chem Phys 116:8610–8615

Schrangl P, Reiterer F, Heinemann L, Freckmann G, Re LD (2018) Limits to the evaluation of the accuracy of continuous glucose monitoring systems by clinical trials. Biosensors 18:5001–5023

Schwan HP (1957) Electrical properties of tissue and cell suspensions. In: Lawrence JH, Tobias CA (eds) Advances in biological and medical physics, vol 5. Academic, New York, pp 147–209

Schwan HP (1963) Determination of biological impedances. In: Nastuk WL (ed) Physical techniques in biological research, vol 6. Academic, New York, pp 323–407

Shinyashiki N, Yagihara S, Arita I, Mashimo S (1998) Dynamics of water in polymer matrix studied by a microwave dielectric measurement. J Phys Chem 102:3249–3251

Siegel PH, Lee Y, Pikov V (2014) Millimeter-wave non-invasive monitoring of glucose in anesthetized rats. 39th international conference on infrared, millimeter, and terahertz waves (IRMMW-THz). IEEE, Tucson, Arizona, USA

Siegel PH, Tang A, Virbila G, Kim Y, Chang MCF, Pikov V (2015) Compact non-invasive millimeter-wave glucose sensor. 40th international conference on infrared, millimeter, and terahertz waves (IRMMW-THz). IEEE, Hong Kong, China

Siegel PH, Dai W, Kloner RA, Csete M, Pikov V (2016) First millimeter-wave animal in vivo measurements of L-glucose and D-glucose: further steps towards a non-invasive glucometer. 2016 41st international conference on infrared, millimeter, and terahertz waves (IRMMW-THz). IEEE, Copenhagen

Stokke BT, Mikkelsen A, Elgsaeter A (1986) Spectrin, human erythrocyte shapes, and mechanochemical properties. Biophys J 49:319–327

Suzuki T (2008) The hydration of glucose: the local configurations in sugar–water hydrogen bond. Phys Chem Chem Phys 10:96–105

Takashima S (1989) Electrical properties of biopolymers and membranes. Adam Hilger, Bristol

Talary MS, Dewarrat F, Caduff A, Puzenko A, Ryabov Y, Feldman Y (2006) An RCL sensor measuring dielectrically lossy materials in the MHz frequency range. 1. Comparison of hydrogel model simulation and with actual hydrogel impedance measurements. IEEE Trans Dielect Electric In 13:247–256

Tierney MJ, Tamada JA, Potts RO, Jovanovic L, Garg S, Team CR (2001) Clinical evaluation of the GlucoWatch® biographer: a continual, non-invasive glucose monitor for patients with diabetes. Biosens Bioelectron 16:621–629

van Solinge WW, van Wijk R (2010) Disorders of red cells resulting from enzyme abnormalities. In: Kaushansky K, Lichtman M, Beutler E, Kipps T, Prchal J, Seligsohn U (eds) Williams Hematology

Vashist SK (2012) Non-invasive glucose monitoring technology in diabetes management: a review. Analytica Chimica Acta 750:16–27

Wadwa RP, Laffel LM, Shah VN, Garg SK (2018) Accuracy of a factory-calibrated, real-time continuous glucose monitoring system during 10 days of use in youth and adults with diabetes. Diabetes Technol Ther 20:395–402

Wei YZ, Chiang P, Sridhar S (1992) Ion size effects on the dynamic and static dielectric properties of aqueous alkali solutions. J Chem Phys Eng Data 96:4569–4573

Windmiller JR, Wang J (2013) Wearable electrochemical sensors and biosensors: a review. Electroanalysis 25:29–46

Wolf M, Gulich R, Lunkenheimer P, Loidl A (2011) Broadband dielectric spectroscopy on human blood. Biochim Biophys Acta 1810:727–740

Wolf M, Emmert S, Gulich R, Lunkenheimer P, Loidl A (2015) Dynamics of protein hydration water. Physical Review E 92: 032727–032726

Xiao X, Li Q (2017) A noninvasive measurement of blood glucose concentration by UWB microwave spectrum. IEEE Antenn Wirel Propag Lett 16:1040–1043

Yadav J, Rani A, Singh V, Murari BM (2015) Prospects and limitations of non-invasive blood glucose monitoring using near-infrared spectroscopy. Biomed Signal Process Control 18:214–227

Yan Q, Peng B, Su G, Cohan BE, Major TC, Meyerhoff ME (2011) Measurement of tear glucose levels with amperometric glucose biosensor/capillary tube configuration. Anal Chem 83:8341–8346

Yilmaz T, Foster R, Hao Y (2019) Radio-frequency and microwave techniques for non-invasive measurement of blood glucose levels. Diagnostics 9:2–34

Zanon M, Sparacino G, Facchinetti A, Talary MS, Caduff A, Cobelli C (2013a) Regularised model identification improves accuracy of multisensor systems for noninvasive continuous glucose monitoring in diabetes management. J Appl Math 2013:10

Zanon M, Sparacino G, Facchinetti A, Talary MS, Mueller M, Caduff A, Cobelli C (2013b) Non-invasive continuous glucose monitoring with multi-sensor systems: a Monte Carlo-based methodology for assessing calibration robustness. Sensors 13:7279–7295

Zanon M, Mueller M, Zakharov P, Talary MS, Donath M, Stahel WA, Caduff A (2018) First experiences with a wearable multisensor device in a noninvasive continuous glucose monitoring study at home, part II: the investigators' view. J Diabetes Sci Technol 12:554–561

Zhang R, Liu S, Jin H, Luo Y, Zheng Z, Gao F, Zheng Y (2019) Noninvasive electromagnetic wave sensing of glucose. Sensors 19: 1151–1120

Zuo S, Hellman U, Lundahl P (2003) On the oligomeric state of the red blood cell glucose transporter GLUT1. Biochim Biophys Acta 1618:8–16